AD-A105 198 ADVANCED RESEARCH AND APPLICATIONS CORP SUNNYVALE CA F/G 13/8
SILICON QUALITY: A CONSIDERATION FOR VHSI CIRCUIT DEVELOPMENT.(U)
SEP 81 T J MAGEE, C LEUNG, R ORMOND N00014-80-C-0071
UNCLASSIFIED ARACOR-FR-81-53 NL

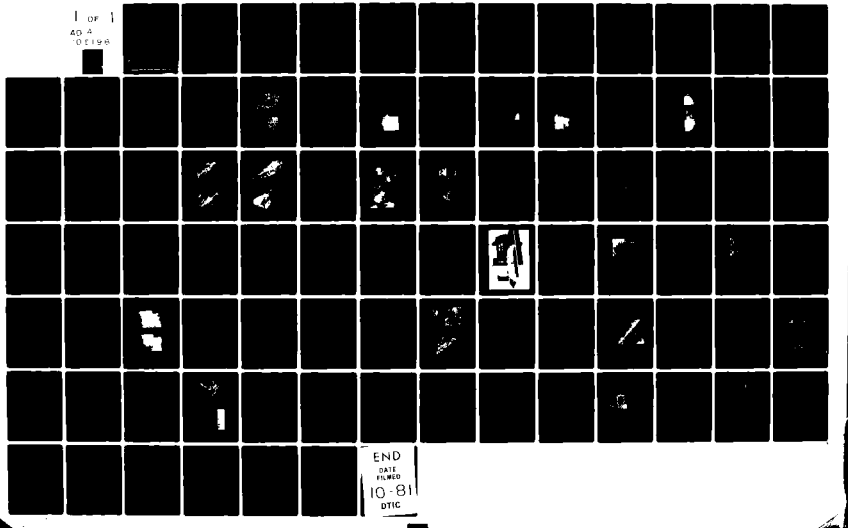

ARACOR

SILICON QUALITY:
A CONSIDERATION FOR VHSI CIRCUIT DEVELOPMENT

FINAL REPORT

BY

T. J. MAGEE

PREPARED FOR:

OFFICE OF NAVAL RESEARCH
DEPARTMENT OF THE NAVY
800 NORTH QUINCY STREET
ARLINGTON, VIRGINIA 22217

ATTN: MR. M. N. YODER,
CODE 427

FINAL REPORT FR-81-53

ADVANCED RESEARCH AND APPLICATIONS CORPORATION

UNCLASSIFIED
SECURITY CLASSIFICATION OF THIS PAGE (When Data Entered)

REPORT DOCUMENTATION PAGE

READ INSTRUCTIONS BEFORE COMPLETING FORM

1. REPORT NUMBER: FR 81-53
2. GOVT ACCESSION NO.: AD-A105198
3. RECIPIENT'S CATALOG NUMBER:

4. TITLE (and Subtitle): SILICON QUALITY: A CONSIDERATION FOR VHSI CIRCUIT DEVELOPMENT
5. TYPE OF REPORT & PERIOD COVERED: Final Report, 15 Dec 1979 - 15 Sept 1981
6. PERFORMING ORG. REPORT NUMBER:

7. AUTHOR(s): T. J. Magee, C. Leung, R. Ormond and L. J. Palkuti
8. CONTRACT OR GRANT NUMBER(s): N00014-80-C-0071

9. PERFORMING ORGANIZATION NAME AND ADDRESS:
Advanced Research and Applications Corporation
1223 East Arques Avenue
Sunnyvale, California 94086

10. PROGRAM ELEMENT, PROJECT, TASK AREA & WORK UNIT NUMBERS:

11. CONTROLLING OFFICE NAME AND ADDRESS:
Office of Naval Research
Code 427 (Mr. Yoder)
Arlington, VA 22217

12. REPORT DATE: Sept. 28, 1981
13. NO. OF PAGES: 80

14. MONITORING AGENCY NAME & ADDRESS (if diff. from Controlling Office):

15. SECURITY CLASS. (of this report): UNCLASSIFIED

15a. DECLASSIFICATION/DOWNGRADING SCHEDULE:

16. DISTRIBUTION STATEMENT (of this report)
Approved for public release; distribution unlimited.

17. DISTRIBUTION STATEMENT (of the abstract entered in Block 20, if different from report)

18. SUPPLEMENTARY NOTES
ONR Scientific Officer
Telephone: (202) 696-4218

19. KEY WORDS (Continue on reverse side if necessary and identify by block number)

Silicon	Stacking Faults	Reliability	Silicon Growth
VHSIC	Gettering	Device Processing	Wafer Warpage
VLSIC	Oxygen Diffusion	Infrared Absorption	Impurity Effects
Defects	Semiconductors	Enhanced Diffusion	

20. ABSTRACT (Continue on reverse side if necessary and identify by block number)

A detailed evaluation of the quality of silicon wafers from representative domestic and foreign vendors was made. To avoid pre-selection of wafers by vendors, material was obtained directly from device manufacturers and therefore represents a statistical sampling of Si material as currently being used in production-line processing. The results of this study have shown extreme batch-to-batch variability, lack of control in material quality and, in many cases, unacceptable levels of defects in silicon wafers used in manufacturing.

DD FORM 1 JAN 73 1473
EDITION OF 1 NOV 65 IS OBSOLETE

The development of front-and-back-surface laser-gettering procedures for improving quality is reported and newly developed techniques for stabilizing back-surface damage, using the enhanced diffusion of oxygen, are discussed.

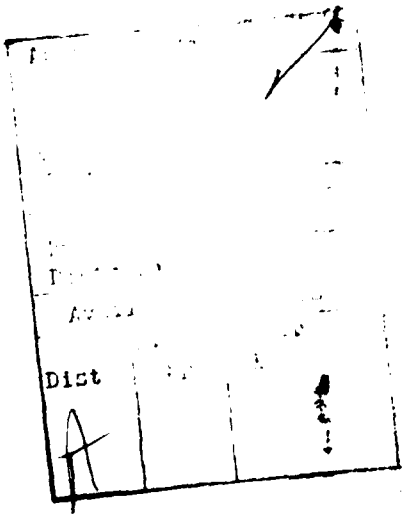

CONTENTS

FIGURES

TABLES

1. INTRODUCTION

The Department of Defense (DoD) has embarked upon a major new initiative in very-large-scale integrated (VLSI) circuits. The general goal of this program is to advance semiconductor microcircuit technology for military applications, with primary emphasis on achieving a significant increase both in functional capacity and device operating speed. Since throughput, not circuit element density alone, is the objective, this activity has been designated the very-high-speed integrated circuits, or VHSIC, program.

Although the evaluation of the quality of commercial silicon (Si) and improving it, if necessary, is not listed as a separate program area, it has been recognized that the desired higher levels of circuit integration and circuit element miniaturization will require a greater sophistication in defect control. It is possible that limitations in yield and circuit performance due to native and process-induced defects may prove to be a significant factor in the attainment of proposed near- and long-term goals. Reductions in defect and impurity levels should also contribute to radiation hardness, which is a secondary objective of the VHSIC program.

A second consideration is the question of whether the quality of commercial Si is uniform from vendor to vendor and, if not, what unique features are exhibited by wafers from the various vendors and how these features relate to VHSIC processing. It is also important to determine if there are substantial differences in the characteristics of domestically-produced Si compared to wafers from major foreign sources.

During the period 1978 to 1981, there have been considerable problems encountered on integrated circuit production lines relating to relative device yield/wafer. Many of these yield problems have been directly traced to poor material quality. During this period, the problem appears to have been further accentuated by the excessive market demand over supply, resulting in the utilization of material that would, under other circumstances, have been rejected.

This report addresses the quality of commercial wafers from selected foreign and domestic suppliers. Since the majority of wafers obtained were drawn directly from production line lots, prior to device fabrication, the results obtained in this study reflect the current state of utilization in a number of electronics manufacturing facilities. In the first three sections, we discuss the results obtained regarding oxygen and carbon concentration in silicon wafers used on production lines and, in the latter sections, the use of laser gettering and stabilized back-surface gettering involving the enhanced diffusion of oxygen is discussed. The report does not preclude the use of gettering or control procedures within manufacturing facilities, nor exclude the availability of higher quality material from suppliers, but simply reports the results of wafer sampling from a large number of manufacturers, where wafers were drawn directly from processing lines.

2. SUMMARY OF EXPERIMENTAL PROCEDURES

During the course of this research program, ARACOR evaluated approximately 1200 Si wafers obtained from 16 foreign and domestic suppliers, including both float-zone (FZ) and Czochralski (CZ) material of (111) and (100) orientation and with varying resistivity levels. A partial list of participants in this study is given in Table 1; organizations supplying Si wafers for these investigations are listed in Table 2.

Upon receipt, Si wafers from manufacturers or suppliers were first carefully examined using optical and infrared microscopy to identify "cosmetic" or obvious flaws before additional testing. Wafers containing serious scratches or inclusions were either excluded from testing or set aside for further evaluation.

After suitable cleaning, portions of wafers were subjected to Dash or Sirtl etches to produce dislocation etch pits at the surface. Optical microscopy was then used to determine dislocation densities in as-received materials. Our results showed variable dislocation densities in the range, $<10^2$ to $5 \times 10^3/cm^2$. Most of the wafer lots had previously gone through in-coming screening tests at the manufacturer's facilities and, we found that our results were generally consistent with data obtained by the device manufacturers.

To evaluate initial O and C concentrations in as-received wafers, we used Fourier transform infrared absorption techniques and ASTM procedures.[1] In separate tests, secondary ion mass spectrometry (SIMS) profiles of oxygen

TABLE 1. LIST OF PARTICIPANTS/DEVICE MANUFACTURERS SUPPLYING SILICON FOR RESEARCH PROGRAM.

- ADVANCED MICRODEVICES INC.
- AMERICAN MICROCIRCUITS INC.
- NATIONAL SEMICONDUCTOR
- HITACHI
- MATSHUSHITA INC.
- ZILOG
- SYNERTEK
- INTEL
- TOSHIBA
- NAVAL RESEARCH LABS
- SILTEC
- NBK
- FOUR PHASE SYSTEMS

TABLE 2. LIST OF SILICON SUPPLIERS REPRESENTED IN THIS STUDY.

- O SEMIMETALS
- O SILTEC
- O SILICON MATERIALS (AMETEK)
- O MONSANTO
- O WACKER
- O SMIEL
- O SEH (JAPAN)
- O SEH AMERICA (MALAYSIA)
- O TEXAS INSTRUMENTS
- O NBK
- O TOSHIBA CERAMICS
- O JAPAN SILICON
- O MOTOROLA
- O PCA
- O OSAKA TITANIUM
- O SILICON SUBSTRATES INC.

concentration were determined using a Cameca IMS-3f ion microanalyzer. To establish calibration standards and detection limits for ^{16}O, a controlled oxygen implant was made. The resulting SIMS profiles were then matched against the established chemical profiles and a detection limit of $\leq 3 \times 10^{17}$ atoms/cm^3 determined for ^{16}O in Si.

Wet oxidations were typically done at 1050 to 1100°C for 3 hrs., normally followed by a "dry" anneal for 45 min. to 3 hrs. In all cases, prior to oxidation, the tube furnace was purged overnight with HCl gas to remove excess impurities and contamination and subsequently flushed with streaming Ar. Wafer withdrawal rates in separate experiments, were 1.5 cm/min and 4 cm/min.

After removal of wafers from the furnace, oxide layers were stripped and the wafers subjected to a modified Secco etch[2] [(100) wafers] etch or Sirtl etch[3] [(111) wafers]. The resulting etch figures were then examined by optical or scanning electron microscopy.

Transmission electron microscopic (TEM) analysis of as-received, oxidized or annealed wafers was performed in both bright-and dark-field imaging modes on horizontally-or vertically-sectioned Si wafers. Internal precipitation was examined using vertically-sectioned wafers.

Wafer warpage tests were conducted on samples (containing variable oxygen concentrations) after a series of heat cycle tests at 1050°C for 1 to 100 hrs. Laser interferometry was then used to establish the maximum warpage after each heat cycle.[4] To assess the efficiency of back-surface gettering procedures, both mechanically-induced (abrasion, spiral patterning) and laser-induced damage introduction procedures were examined. Ion-implantation gettering was excluded from

consideration because of the lack of thermal stability and pronounced "reverse" (impurity degettering) annealing characteristics.

Laser irradiations were performed on the ARACOR-scanning CW argon laser annealing system.[5] Wafer temperatures were maintained in the range, 20°C to 300°C, and beam spot sizes were typically 50 to 100 μm in diameter, scan speeds of were the order of 10 to 17 cm/sec.

3. THE EVALUATION OF SILICON QUALITY

3.1 OXIDATION-INDUCED DEFECTS AND SUBSTRATE QUALITY

In a series of tests on 900 samples, we subjected Si wafers of (100) and (111) orientation to a wet oxidation at 1100°C for 3.75 hrs., followed by dry oxidation for 1.25 hrs., in a three-zone furnace.

Upon completion of the oxidation, wafers were taken from the furnace and immersed in an HF solution to remove oxide layers. The samples were then etched either in a Sirtl (111) or modified Secco (100) solution for 10 to 15 minutes to reveal etch figures on the Si surfaces.

In Figs. 1-5, we show representative optical micrographs of Si wafers from a number of suppliers. In Fig. 1, we observe an extremely high concentration of oxidation-induced stacking faults (OSF) with substantial development of pitting along the length of the OSF in these wafers (Wacker). The presence of these pits suggested that the OSF could be correlated with the presence of precipitates (PCI) nucleated during the annealing. To further investigate the OSF/PCI correlation, we immersed samples in HF solutions for variable periods after oxide removal. It was found that pits were enlarged after a period of immersion, reaching a saturation size limit after 15 minutes of exposure. The results suggested that the PCI were a form of SiOx and that the OSF development was related to PCI formation and oxygen content, as has been proposed in a number of earlier publications. Correlated TEM analysis of wafers from this batch lot confirmed that the PCI were a form of SiOx, as will be discussed in a subsequent section.

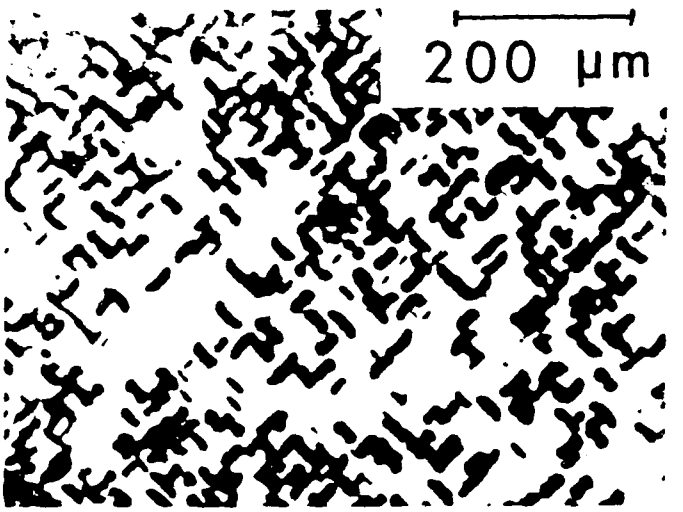

(a)

(b)

FIG. 1. OPTICAL MICROGRAPHS OF SILICON SURFACES AFTER OXIDATION AND ETCHING-WCZ (100); a) WACKER, CZ (100), P-TYPE, 6.9-9.0 Ω-CM; b) WACKER, CZ, (100), P-TYPE, 6.9-9.0 Ω-CM, EXTENDED IMMERSION IN HF SOLUTION AFTER SECCO ETCH.

In contrast to the previous results, wafers obtained from Smiel consistently showed a lower concentration of OSF (Fig. 2) than Wacker wafers. Separate wafer lots from Wacker also showed considerably reduced OSF densities, implying some variability in Si growth conditions by the same manufacturer.

In Figs.3-5, we show additional micrographs obtained after oxidation and etching, illustrating the extreme variability on both (100) and (111) wafers from different vendors or the same vendor in separate samples from other boules. For reference, a brief summary of representative data obtained from various wafers is listed in Table 3.

In Fig.6, we show optical micrographs obtained from a Monsanto and Shinetsu wafer after oxidation and etching. In both cases, the wafers contained relatively-low levels of oxygen and exhibited relatively-low OSF densities. In Fig.7, we show optical micrographs obtained on wafers from Japanese suppliers, illustrating the dependence of OSF density on oxygen concentration (19-40 ppm oxygen). In general, we observed a more consistent quality in wafers from batch lots obtained from Shinetsu. Wafers from Monsanto, Siltec, NBK and Wacker showed extreme variability from lot to lot, although a number of wafers were considered acceptable.

Of particular importance for this study is the observation of extreme lateral variations in OSF densities across the surface of wafers, reflecting the non-uniform incorporation of oxygen or other impurities during growth. Of all wafers tested, the Shinetsu samples (19-25 ppm oxygen) exhibited the most laterally uniform concentration of OSFs. This is believed to be the result, in part, of improved growth techniques for reducing eddy currents and/or controling thermal gradients. Since non-uniform oxygen

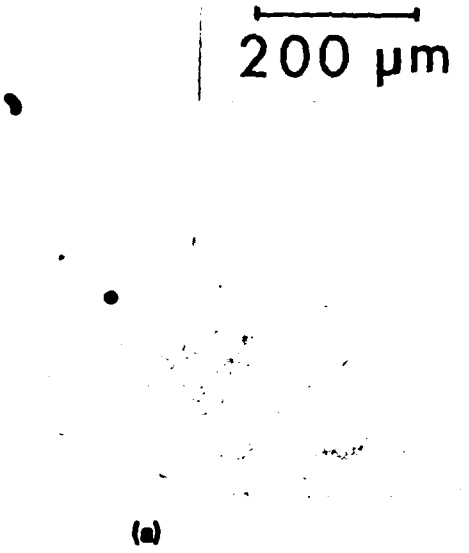

(a)

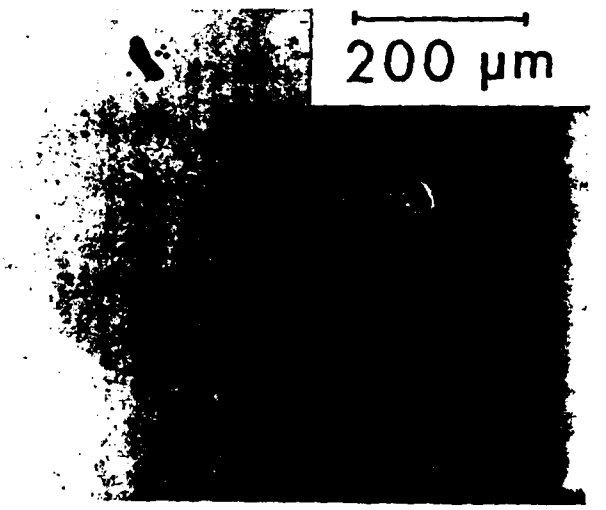

(b)

FIG. 2. OPTICAL MICROGRAPHS ON SILICON SURFACES AFTER OXIDATION AND ETCHING SMLCZ (100); SMIEL, CZ, (100), N-TYPE, 6.9-9.0 Ω-CM.

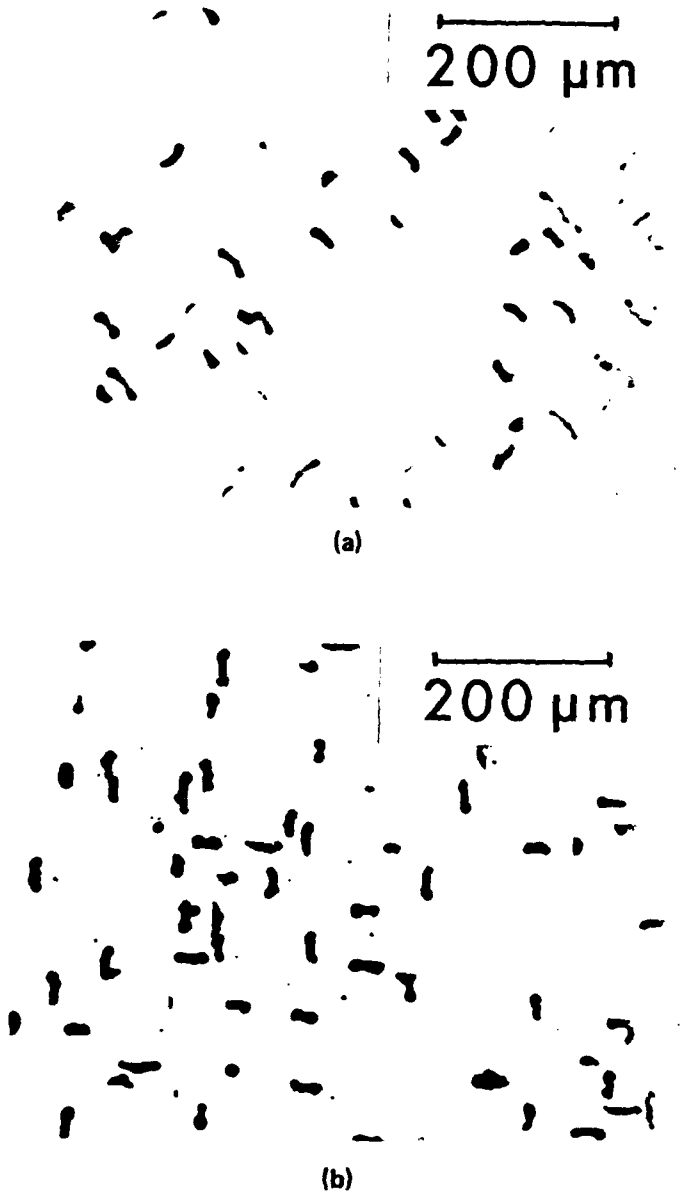

FIG. 3. OPTICAL MICROGRAPHS OF SILICON SURFACES AFTER OXIDATION AND ETCHING - NBKCZ (100); NBK, CZ, (100), N-TYPE, 1.0-5.0 Ω-CM.

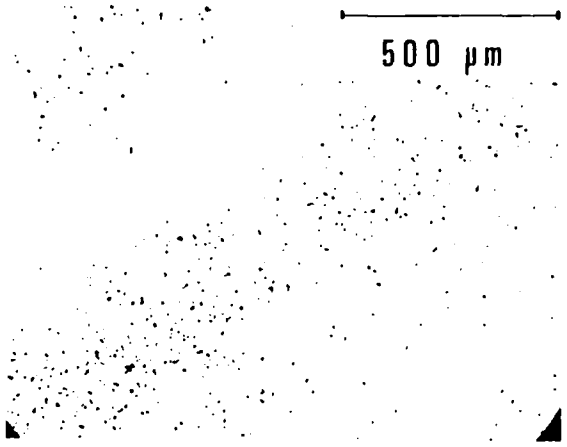

(a)

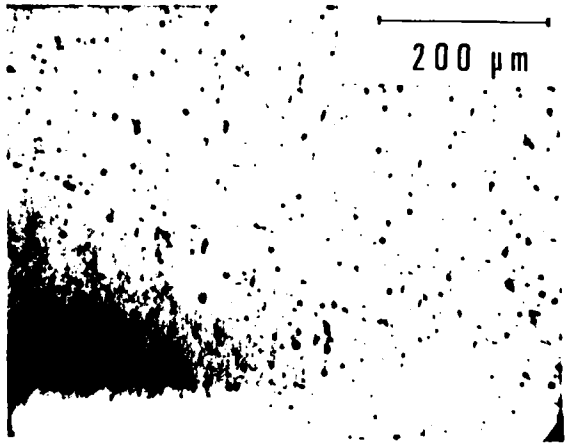

(b)

FIG. 4. OPTICAL MICROGRAPHS OF SILICON SURFACES AFTER OXIDATION AND ETCHING - NBKCZNP (100); a) NBK, CZ, (100), N-TYPE, (100), N-TYPE, 10-20 Ω-CM; b) NBK, CZ (100), P-TYPE, 10-20 Ω-CM.

(a)

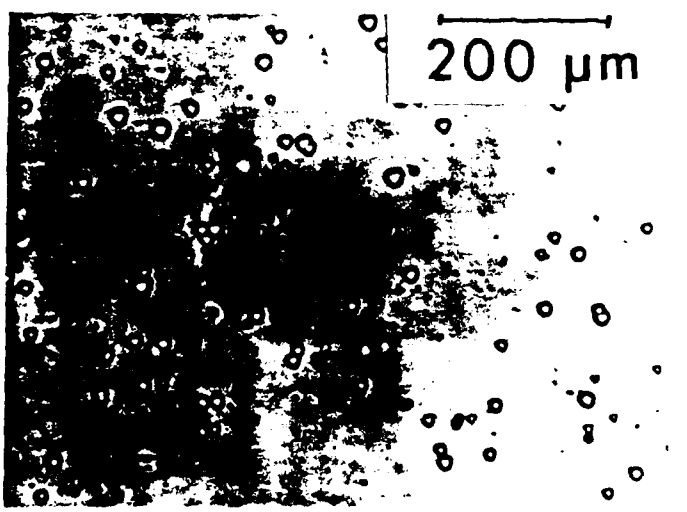

(b)

FIG. 5. OPTICAL MICROGRAPHS OF SILICON SURFACES AFTER OXIDATION AND ETCHING - NBKCZ (100); NBK, CZ, (111), N-TYPE, 5-10 Ω-CM.

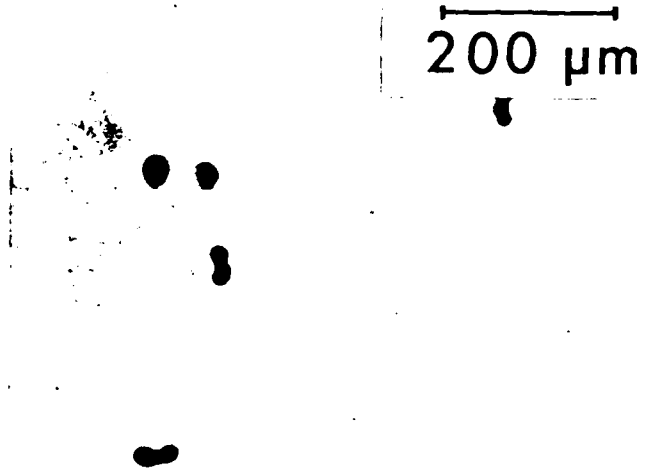

(a)

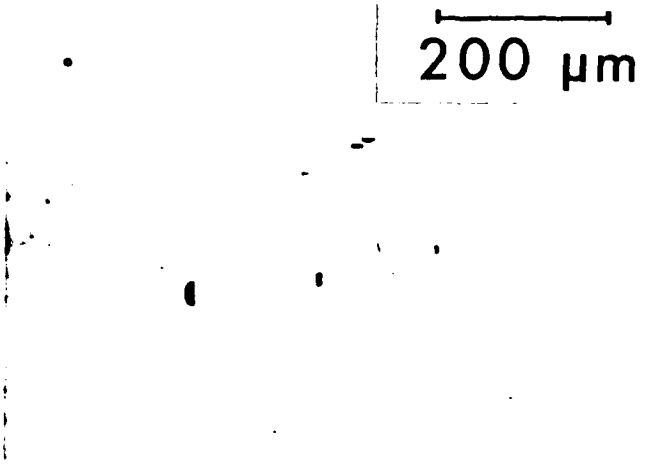

(b)

FIG. 6. OPTICAL MICROGRAPHS OF SILICON SURFACES AFTER OXIDATION AND ETCHING-MON-SHIN-CZ (100); a) MONSANTO, CZ, N-TYPE, 21 PPM OXYGEN; b) SHINETSU, CZ, N-TYPE, 19 PPM OXYGEN.

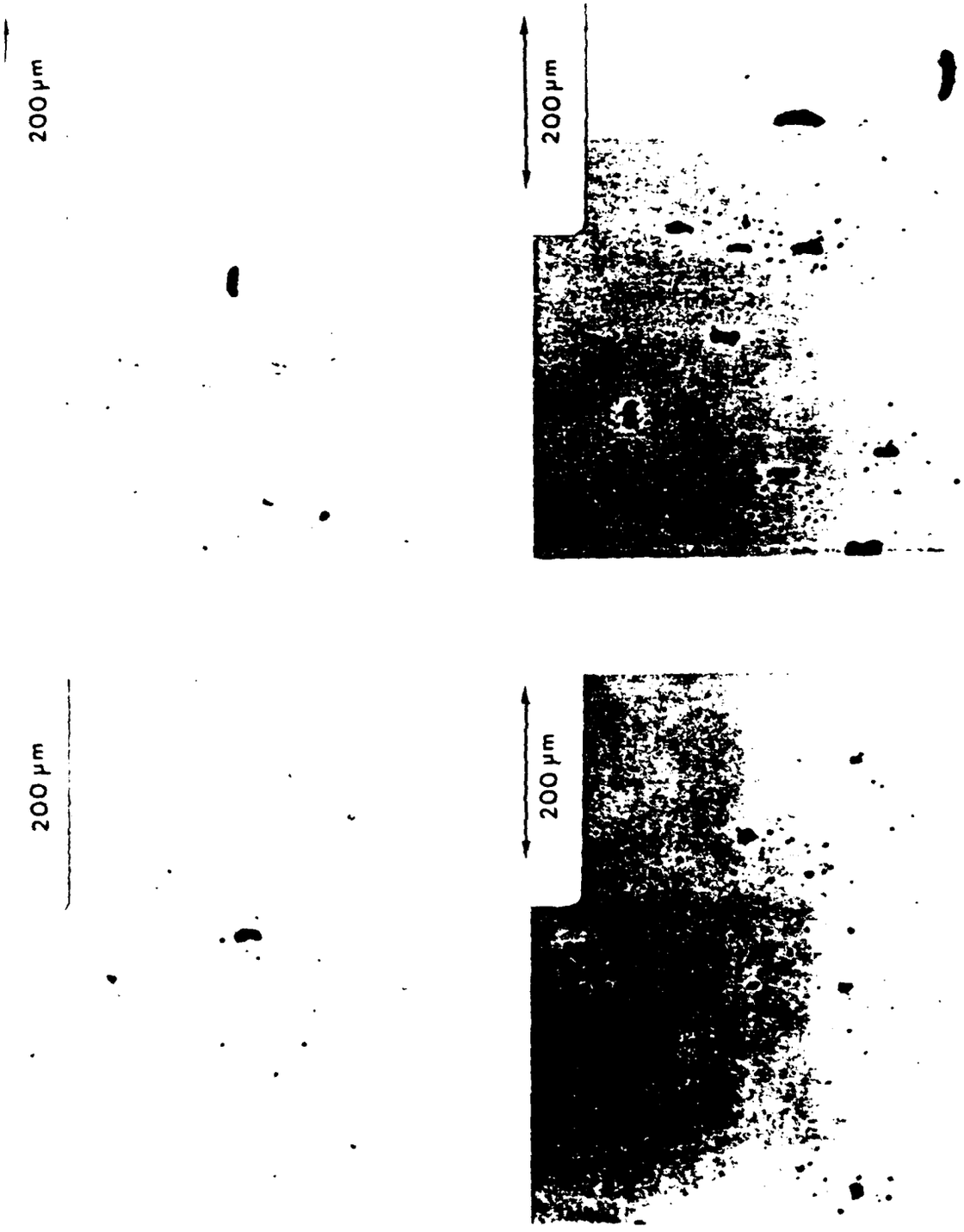

FIG. 7. OPTICAL MICROGRAPHS OF SILICON SURFACES AFTER OXIDATION AND ETCHING (JAPANESE MATERIAL SUPPLIERS) SHOWING THE EFFECT OF VARIABLE OXYGEN CONCENTRATION.

TABLE 3. REPRESENTATIVE DATA OBTAINED ON SILICON WAFERS

Sample	Source	Orient	Growth	Type/ Resistivity	(Ω-cm)	Oxidation	Etchant	Etch Figure Density (cm^{-2})
AR221801A	NBK	(111)	CZ	N-	5-10	A	Sirtl	1.79 (10^4)
AR221801B	NBK	(111)	CZ	N-	5-10	A	Sirtl	8.57 (10^4)
AR221801G	NBK	(111)	CZ	N-	5-10	A	Sirtl	3.21 (10^4)
AR222803A	NBK	(111)	Ct	N-	5-10	A	Sirtl	1.43 (10^4)
AR222803A	NBK	(111)	Ct	P-	10-20	A	Sirtl	2.07 (10^2)
AR222803B	NBK	(111)	Ct	P-	10-20	A	Sirtl	4.15 (10^2)
AR222803C	NBK	(111)	Ct	P-	10-20	A	Sirtl	8.30 (10^2)
AR222803D	NBK	(111)	Ct	P-	10-20	A	Sirtl	4.15 (10^2)
AR221803A	NBK	(100)	CZ	N-	10-20	A	Secco	8.30 (10^2)
AR221803B	NBK	(100)	CZ	N-	10-20	A	Secco	1.66 (10^3)
AR221803C	NBK	(100)	CZ	N-	10-20	A	Secco	4.29 (10^3)
AR221803D	NBK	(100)	CZ	N-	10-20	A	Secco	1.25 (10^3)
AR221802A	NBK	(100)	CZ	P-	10-20	A	Secco	4.15 (10^2)
AR221802B	NBK	(100)	CZ	P-	10-20	A	Secco	1.04 (10^3)
AR221802C	NBK	(100)	CZ	P-	10-20	A	Secco	1.04 (10^3)
AR221802D	NBK	(100)	CZ	P-	10-20	A	Secco	2.07 (10^3)
AR303801A	Wacker	(100)	CZ	P-	6- 9.9	A	Secco	2.57 (10^5)
AR303801B	Wacker	(100)	CZ	P-	6- 9.9	A	Secco	2.86 (10^5)
AR303801C	Wacker	(100)	CZ	P-	6- 9.9	A	Secco	1.71 (10^5)
AR303801D	Wacker	(100)	CZ	P-	6- 9.9	A	Secco	2.57 (10^5)
AR311801A	Wacker	(111)	CZ	N-	3.5- 5.0	A	Sirtl	1.04 (10^3)
AR311801B	Wacker	(111)	CZ	N-	3.5- 5.0	A	Sirtl	8.30 (10^2)
AR311801C	Wacker	(111)	CZ	N-	3.5- 5.0	A	Sirtl	2.07 (10^2)

Sample	Source	Orient	Growth	Type/ Resistivity	(Ω-cm)	Oxidation	Etchant	Etch Figure Density (cm^{-2})
AR310802A	Wacker	(111)	CZ	N-	6- 9.9	A	Sirtl	$<10^2$
AR310802B	Wacker	(111)	CZ	N-	6- 9.9	A	Sirtl	1 (10^5)
AR310802C	Wacker	(111)	CZ	N-	6- 9.9	A	Sirtl	$<10^2$
AR311802A	Monsanto	(111)	CZ	N-	4- 5	A	Sirtl	6.22 (10^2)
AR311802B	Monsanto	(111)	CZ	N-	4- 5	A	Sirtl	4.15 (10^2)
AR311802C	Monsanto	(111)	CZ	N-	4- 5	A	Sirtl	1.25 (10^3)
AR311803A	Monsanto	(100)	CZ	P-	7- 9	A	Secco	6.22 (10^2)
AR311803B	Monsanto	(100)	CZ	P-	7- 9	A	Secco	6.22 (10^2)
AR311803C	Monsanto	(100)	CZ	P-	7- 9	A	Secco	4.15 (10^2)
AR303802A	Smiel	(100)	CZ	P-	6- 9.9	A	Secco	6.22 (10^2)
AR303802B	Smiel	(100)	CZ	P-	6- 9.9	A	Secco	4.15 (10^2)
AR303802C	Smiel	(100)	CZ	P-	6- 9.9	A	Secco	6.22 (10^2)
AR303802D	Smiel	(100)	CZ	P-	6- 9.9	A	Secco	4.15 (10^2)
AR314802A	Shinetsu	(100)	CZ	P-	0.8- 1.2	A	Secco	$<10^2$
AR314802B	Shinetsu	(100)	CZ	P-	4- 6	A	Secco	1.2 (10^2)
AR314802C	Shinetsu	(100)	CZ	P-	9- 11	A	Secco	$<10^2$
AR314802D	Shinetsu	(100)	CZ	P-	10- 15	A	Secco	$<10^2$
AR315802A	Japan Si	(100)	CZ	N-	10- 15	A	Secco	1.2 (10^3)
AR316802A	Osaka Ti	(100)	CZ	P-	10- 15	A	Secco	4 (10^2)
AR316802B	Osaka Ti	(100)	CZ	P-	10- 15	A	Secco	1 (10^2)
AR318801A	Toshiba Ceramics	(100)	CZ	P-	6- 10	A	Secco	2.1 (10^3)

Sample	Source	Orient	Growth	Type/ Resistivity	(Ω-cm)	Oxidation	Etchant	Etch Figure Density (cm^{-2})
AR320880A	TI	(100)	CZ	N-	5- 10	A	Secco	7 (10^2)
AR320880B	TI	(100)	CZ	N-	5- 10	A	Secco	2 (10^3)
AR320880C	TI	(100)	CZ	N-	5- 10	A	Secco	5 (10^3)
AR321880A	Siltec	(100)	CZ	N-	5- 10	A	Secco	4 (10^2)
AR321880B	Siltec	(100)	CZ	N-	5- 10	A	Secco	1 (10^3)
AR321880C	Siltec	(100)	CZ	N-	5- 10	A	Secco	1.2 (10^2)

incorporation will produce enhanced wafer deformation during annealing, non-uniform defect nucleation and sporadic device yield variations, it is presently felt that improvements in growth procedures will be required for future VHSIC applications.

To improve the quality of available Si, it has been reported that 2-stage annealing in a nitrogen or argon ambient will reduce the OSF density at the front surface and produce internal SiOx precipitation for gettering. Although TEM examinations indeed confirmed the internal nucleation of SiOx, we did not observe any sizeable reductions in OSF densities at the surface in a large number of wafers, although many exhibited the expected defect denudation at the surface. These results are consistent with the findings of Japanese investigators and emphasize the fact that the two-stage anneal for front-surface defect denudation is not effective for all wafers and is indeed dependent upon quality of the initial starting material.

In extended tests of the thermal stability of internal SiOx precipitation, we found that "reverse" annealing or degettering occurs during heat treatment at temperatures >1100°C. At these temperatures, we observe dissolution of the SiOx precipitates and annihilation of the dislocation structure surrounding the SiOx. Since the dislocation structure is primarily responsible for gettering, the loss of these defects releases trapped defects and impurities which then migrate back to the front surface of the wafer. Hence, from these results, effective internal gettering during processing will be temperature and anneal duration limited.

3.2 TEM EXAMINATIONS OF OSF AND PCT/PDC NUCLEATION IN SILICON WAFERS.

Of particular importance in any investigations of defect nucleation in annealed or oxidized wafers is the identification of stacking fault nuclei and the mechanism of OSF formation. It has been proposed that large numbers of dislocations can be introduced in CZ Si wafers by prismatic punching of precipitates that have been hypothesized to be of composition, SiOx. The OSF observed in these samples have been shown to occur in the region of PCT-dislocation complexes and originate from eventual dissociation of loops introduced by prismatic punching of the PCT.

In this study, we examined a large number of samples after oxidation to determine the PCT-dislocation complex/OSF association. In Fig. 8 and 9, we show bright-field transmission electron micrographs of an oxidized sample (AR 303801B) known to contain a high concentration of oxygen ($>10^{18}/cm^3$).

We observe the presence of platelet precipitates associated with an irregular dislocation line structure. This precipitate-dislocation line complexing (PDC) was observed repeatedly in lot samples obtained from the same batch. In Figures 8(a) and 9(a), the higher magnification micrographs indicate that the platelets are of hexagonal morphology and dislocation lines interconnect platelet arrays as a result of stress generated at the periphery of the PCT. In Fig. 9(b), the electron micrograph shows the correlation between the PDC and OSF.

To provide further information on the correlation of OSF and the PCT, we immersed samples in a dilute HF solution,

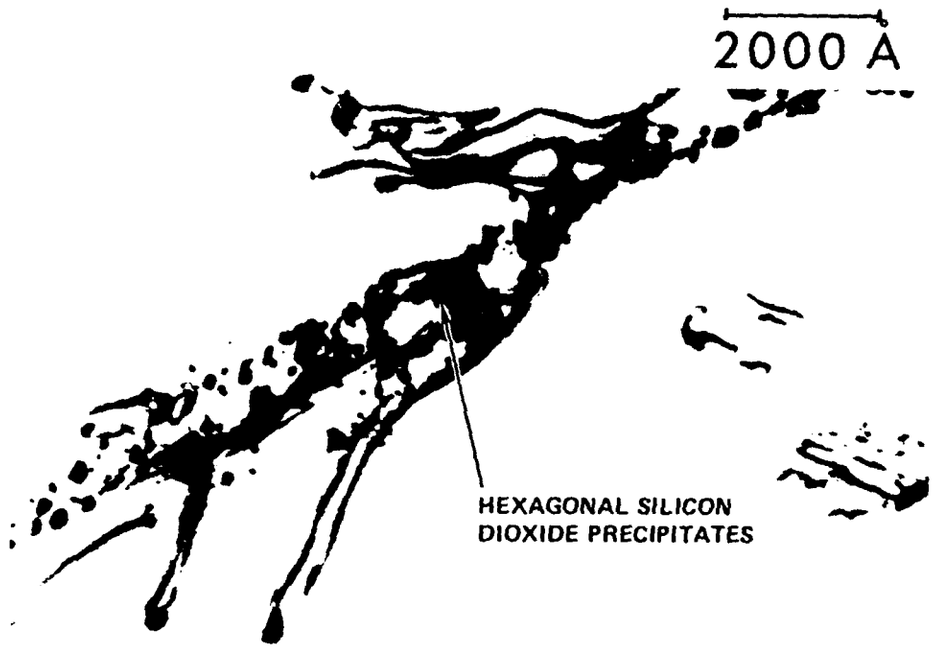

(a)

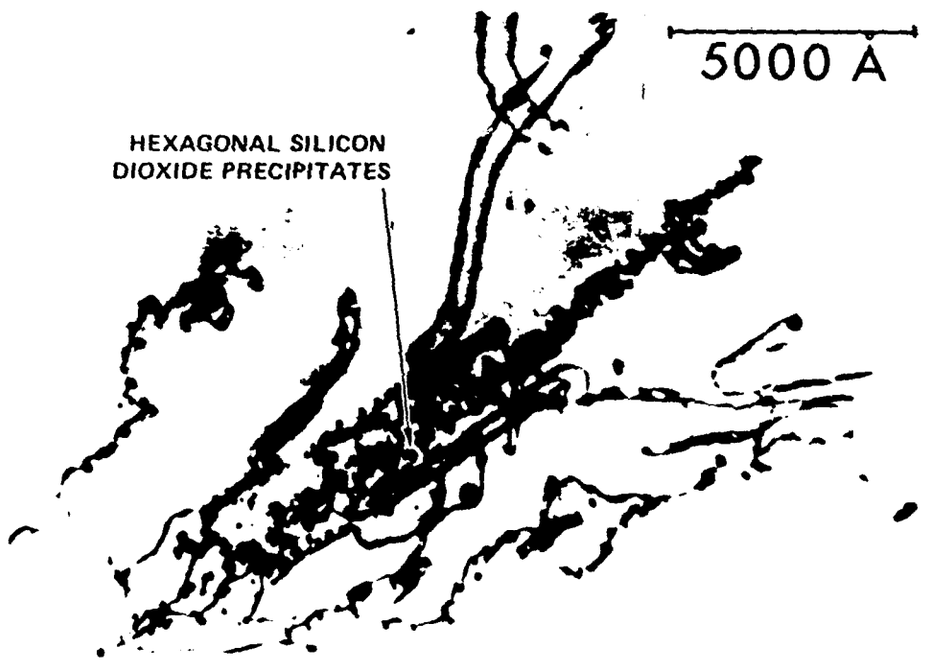

(b)

FIG. 8. TRANSMISSION ELECTRON MICROGRAPHS OF OXIDIZED SILICON SAMPLE CONTAINING HIGH OXYGEN CONCENTRATION AND PDC.

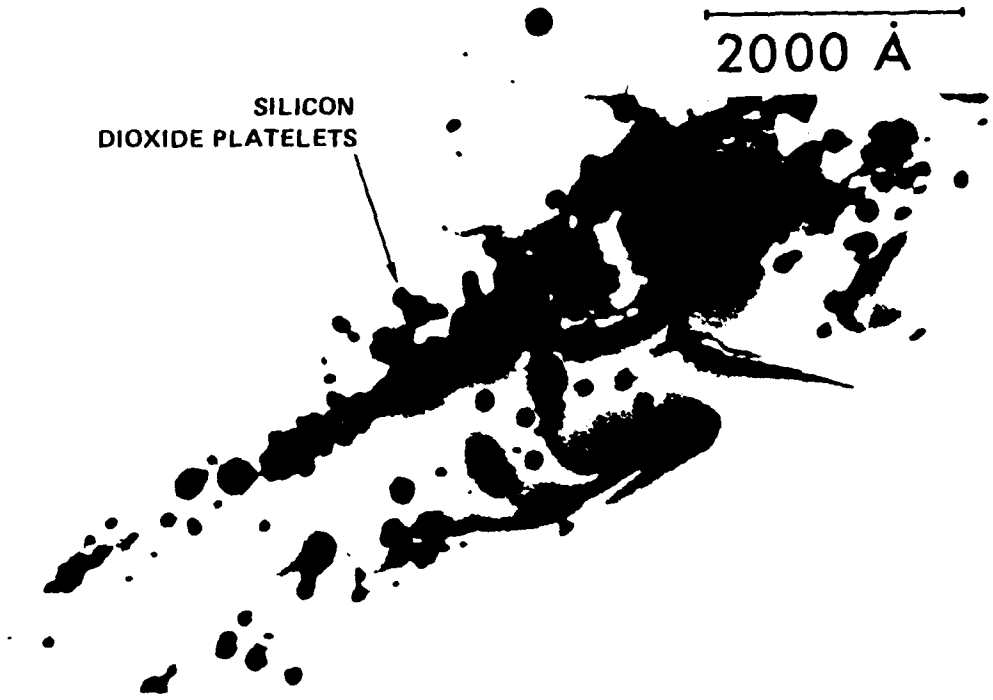

(a)

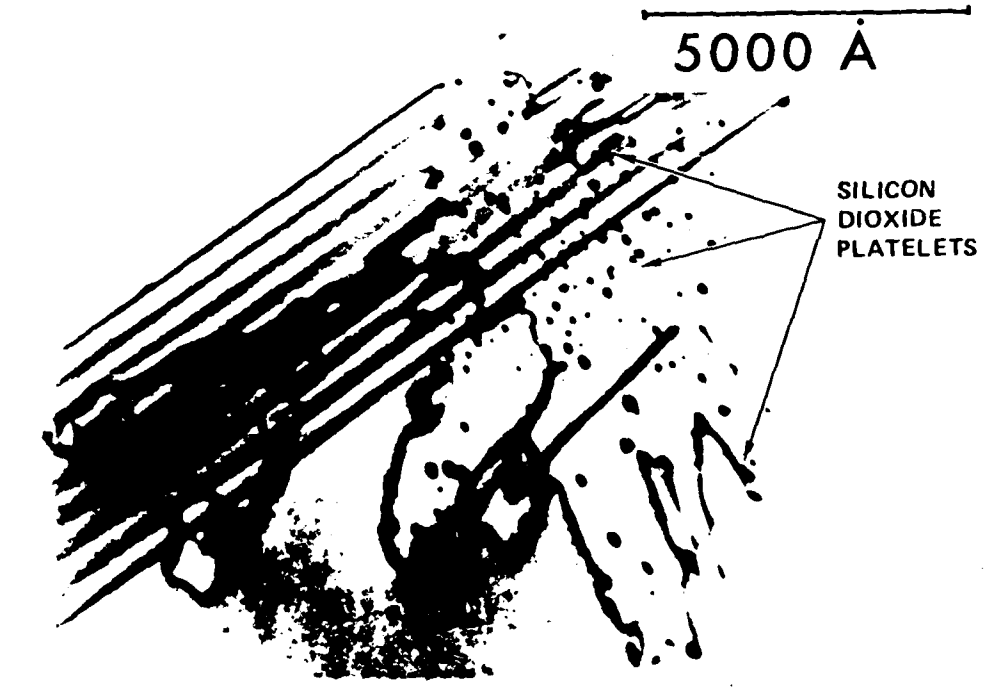

(b)

FIG. 9. TRANSMISSION ELECTRON MICROGRAPHS OF OXIDIZED SILICON SAMPLE CONTAINING HIGH OXYGEN CONCENTRATION; a) HIGH-MAG MICROGRAPH SHOWING SiO_2 PLATELETS ALONG DISLOCATIONS; b) BRIGHT-FIELD MICROGRAPH SHOWING CORRELATION BETWEEN OSF AND PDC.

producing pits along the length of the OSF. The dissolution of the PCT in an HF solution, as well as the presence of a hexagonal habitat on the PCT, suggests that the platelets are indeed composed of SiO_2. The exact composition of the PCT has not been previously determined because of the associated problems in obtaining clear, well-defined diffraction patterns.

To further investigate the role of PDC in defect generation and the correlation with OSF, we obtained wafers intentionally doped with C to levels $\leq$3 ppm. Samples were then annealed at 1100°C for periods of 64 to 100 hrs. in an argon or nitrogen ambient and subsequently examined in the TEM. In these samples, we observed the presence of PCT that were insoluble in HF. In figures 10 and 11, we show bright-field micrographs obtained within the PCT regions. Dislocation lines and extended loops are routinely observed at the sides of the particles, indicative of a prismatic punching effect. In Figure 9(b), we observe a classical distribution of loops generated by the stress around the PCT. In all cases, however, we were unable to identify the composition of the PCT by selected area diffraction, but it is suggested that the particles are a form of silicon carbide.

If, indeed, SiC is formed in the wafers as a result of annealing, the correlation between PDC and OSF will not be limited to the nucleation of SiOx particles, as has been previously hypothesized, but also to SiC-OSF. It will then become important not only to consider the average oxygen concentration or spatial distribution of oxygen, but rather the statistical variations in oxygen-carbon concentration ratio as a parameter in determining OSF densities.

(a)

(b)

FIG. 10. TRANSMISSION ELECTRON MICROGRAPHS OF OXIDIZED SILICON SAMPLE CONTAINING HIGH CARBON CONCENTRATION, ILLUSTRATING THE DEVELOPMENT OF SiC PERCIPITATES AND PDC.

(a)

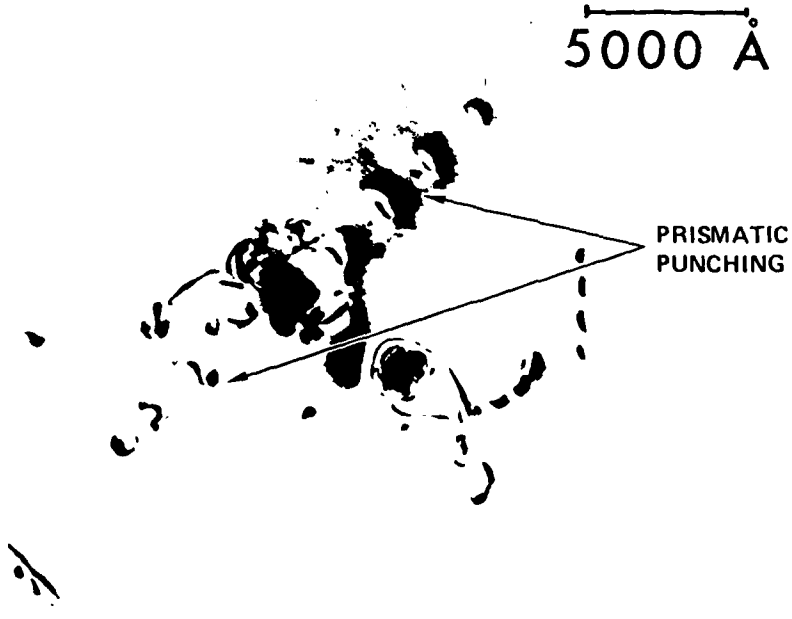

(b)

FIG. 11. TRANSMISSION ELECTRON MICROGRAPHS OF OXIDIZED SILICON WAFERS CONTAINING HIGH CARBON CONCENTRATIONS; a) SiC PRECIPITATE WITH DISLOCATION LINES AT EDGES; b) SiC WITH PRISMATIC PUNCHING OF LOOPS AT EDGE.

3.3 OXYGEN CONTENT AND MICROSTRUCTURAL DEFECT NUCLEATION

To examine the correlation between oxygen content and oxidation-induced defect densities, we subjected wafers from variable lots to wet oxidation at 1100°C for 3.75 hours. After removing the oxide and etching to expose defects, we used optical microscopy to determine defect concentrations. Correlated TEM examinations were also performed to provide confirming data. Average oxygen and carbon concentrations were determined in the same samples from IR absorption measurements prior to oxidation.

In Fig. 12, we show a plot of defect density as a function of initial O concentration for wafers (5 to 10 Ω-cm) obtained from a number of domestic and foreign manufacturers. It is of particular importance to note that the majority of domestic Si contains oxygen in the range, 20 to 40 ppm. Accordingly, the induced defect densities are high and such material would not be acceptable for VHSIC applications. Wafers from Shinetsu (Japan) were consistently low in O concentration and typically showed the lowest defect concentrations after oxidation/annealing.

Similarly, in Fig.13, we observe an apparent linear increase in defect density as a function of oxygen concentrations for wafers of resistivity 1 to 5 Ω-cm. Again, the lowest defect concentrations were observed routinely for Shinetsu (Japan) wafers. To obtain additional information on possible variations in Shinetsu wafers, we made similar measurements on wafers manufactured at various times over a 2-year period (1978-1980). Oxygen concentrations were typically in the range 16 to 21 ppm, with carbon levels < 0.5 ppm. Observed defect densities were $\leq 2/mm^2$, confirming a reasonably consistent control of growth procedures.

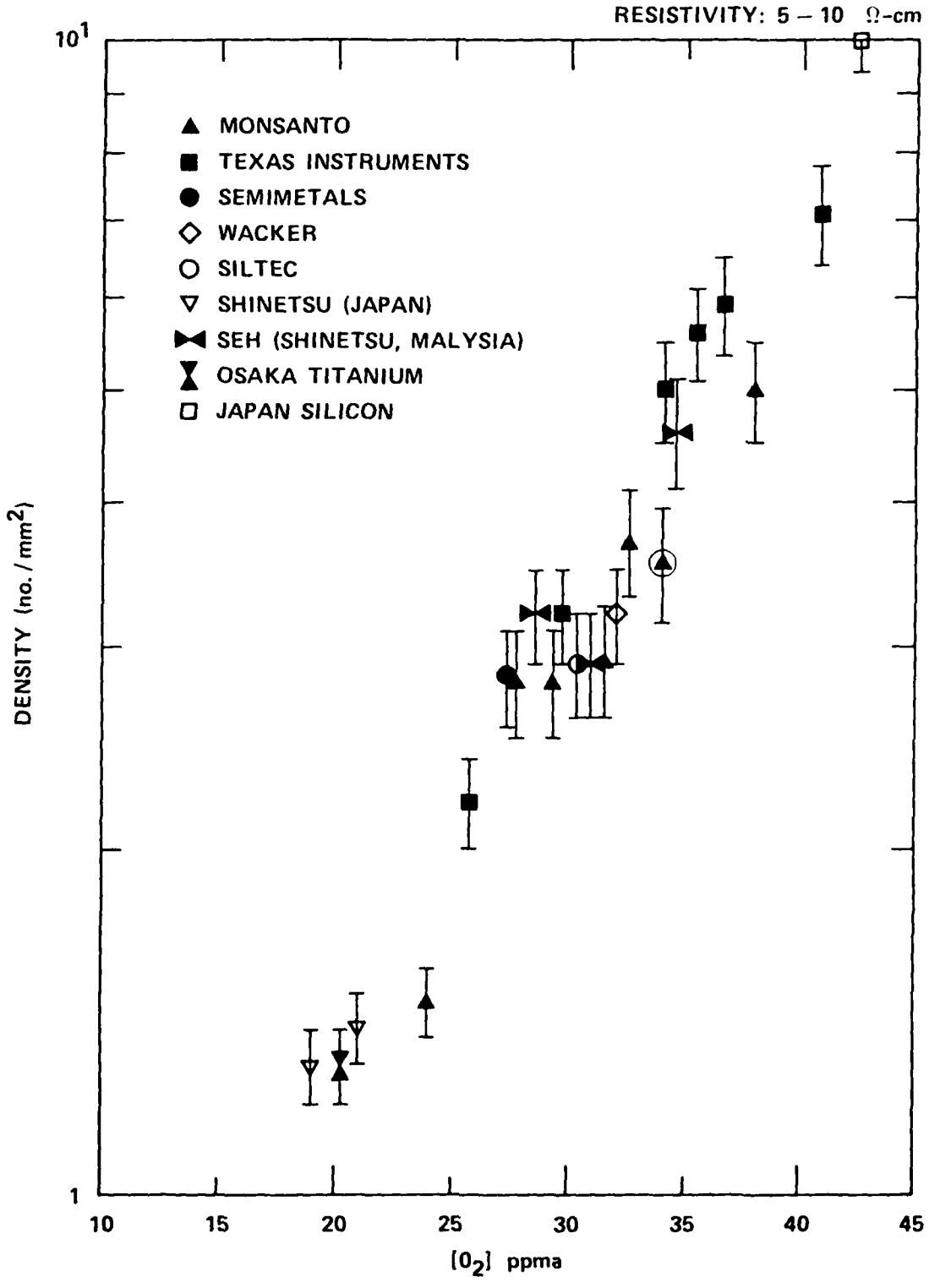

FIG. 12. OXIDATION-INDUCED DEFECT DENSITY IN SILICON WAFERS (5-10 Ω-CM) (U.S., GERMAN AND JAPANESE SUPPLIERS) AS A FUNCTION OF INITIAL OXYGEN CONCENTRATION.

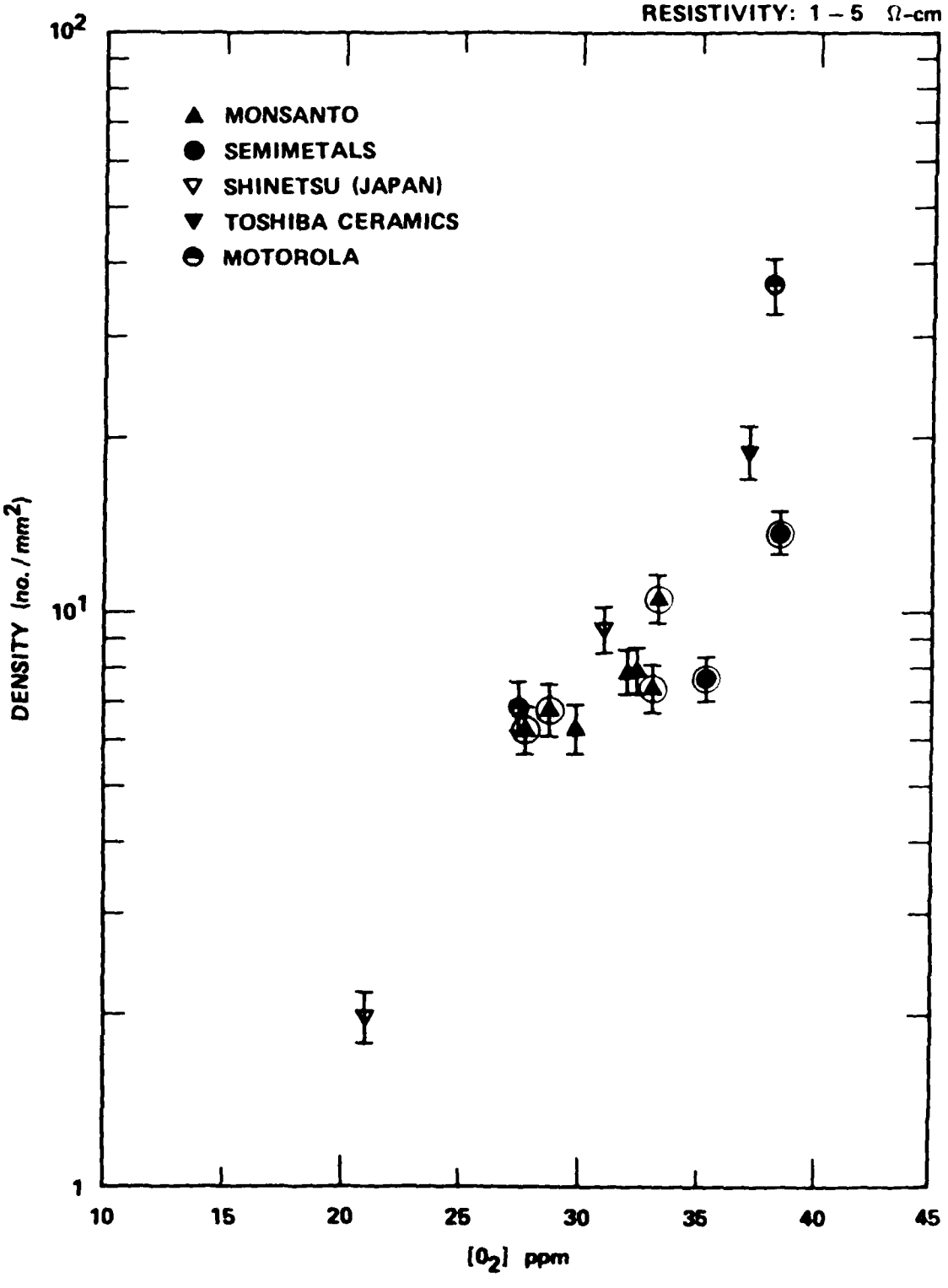

FIG. 13. OXIDATION-INDUCED DEFECT DENSITY IN SILICON WAFERS (1-5 Ω-CM) (U.S. AND JAPANESE SUPPLIERS) AS A FUNCTION OF INITIAL OXYGEN CONCENTRATION.

In Fig. 14, we show comparative data obtained on silicon supplied by domestic and German manufacturers and, correspondingly in Fig. 15, show data obtained on material produced in Japan. In both cases, we observe a similar dependence of defect density on initial oxygen concentration.

From the data obtained on this program, we can conclude that the total oxygen concentration and lateral variation in concentration in much of the currently available silicon may introduce problems in the utilization of materials in VHSIC programs. From available data, we can state that the O concentration should not exceed approximately 30 ppm. Extrapolating the present data, we can postulate that a tolerable range of oxygen in Si for VHSIC program is between 15 and 25 ppm.

3.4 CARBON IN SILICON AND DEFECT NUCLEATION

In the previous section, we have shown that OSF densities in Si wafers increase as a function of increasing oxygen concentration (independent of Si suppliers). In those experiments, the carbon concentration was relatively low ($\leq$ 0.5 ppm) and essentially constant for the samples evaluated. To ascertain whether there might be a correlation between average carbon/oxygen concentration ratio and oxidation-induced defect density at the lower (<25 ppm) oxygen concentrations, a series of (100) wafers were obtained where the boules were intentionally doped with varying concentrations of carbon. Average C and O concentrations were determined using IR absorption. After cleaning, the wafers were subjected to an 1100°C wet oxidation for 3.75 hrs., followed by 1.25 hr. (dry) O_2 anneal at 1050°C. Oxide layers were removed and samples etched in Secco solution. Defect densities were then obtained from optical micrographs of the front surfaces.

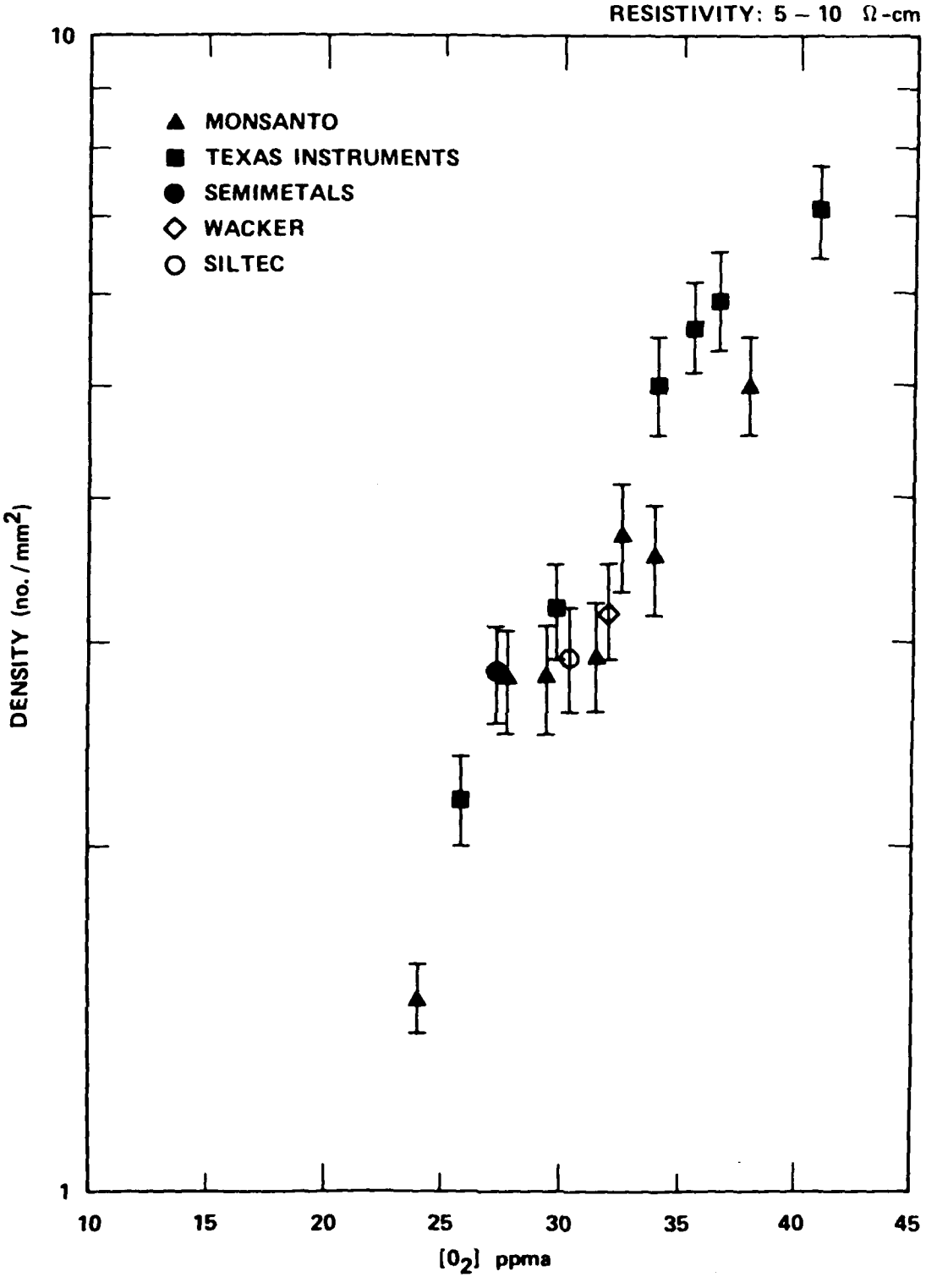

FIG. 14. OXIDATION-INDUCED DEFECT DENSITY IN SILICON WAFERS (5-10 Ω-CM) (U.S. AND GERMAN SUPPLIERS) AS A FUNCTION OF INITIAL OXYGEN CONCENTRATION.

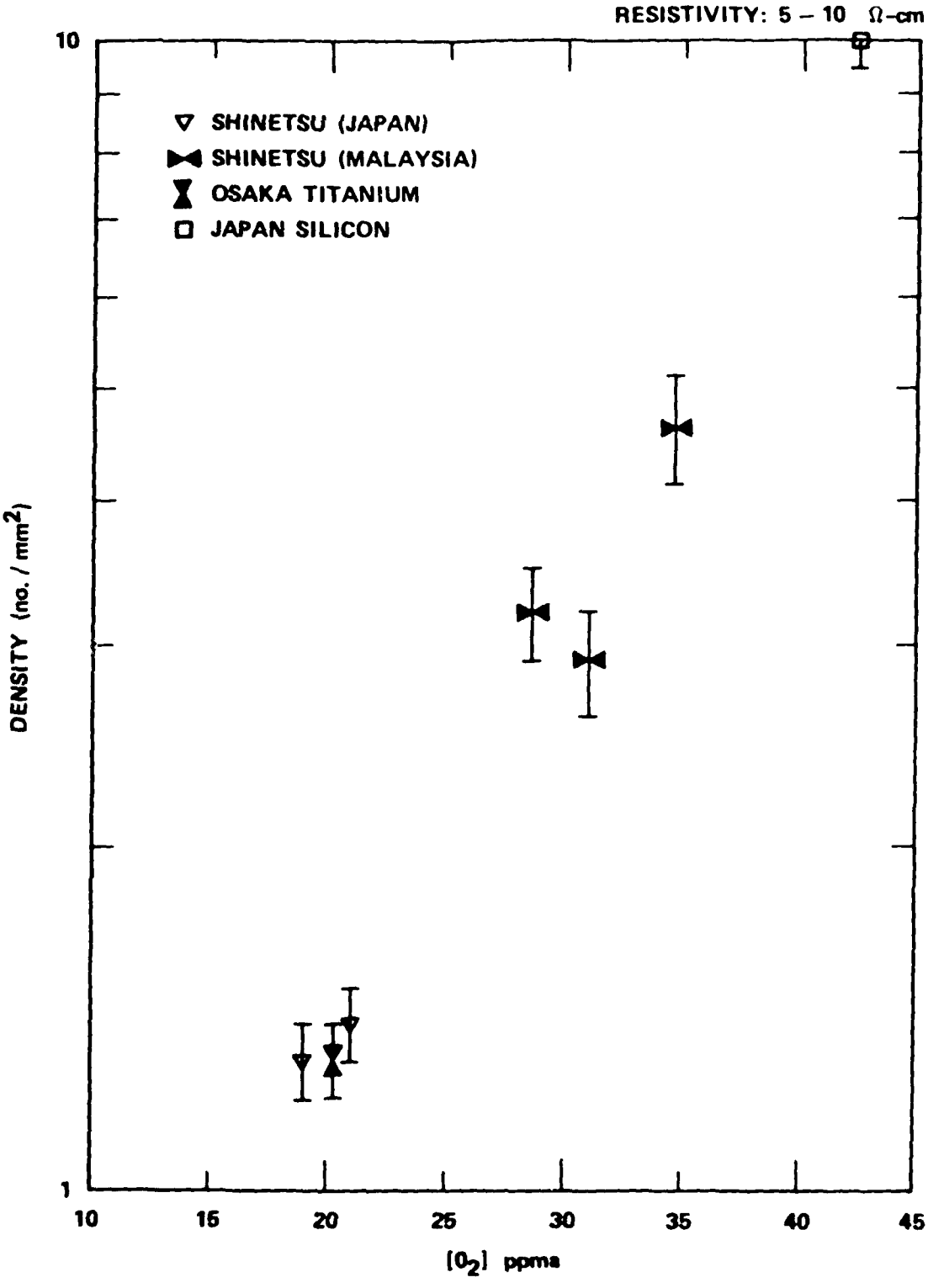

FIG. 15. OXIDATION-INDUCED DEFECT DENSITY IN SILICON WAFERS (5-10 Ω-CM) (JAPANESE SUPPLIERS) AS A FUNCTION OF INITIAL OXYGEN CONCENTRATION.

Table 4 lists the data obtained in these experiments. We observe that the average oxidation-induced defect density increases as a function of increasing oxygen concentration and decreases as a function of increasing carbon concentration. In the fourth and fifth columns of Table 4, the calculated O/C and C/O concentration ratios are listed. Although there is again no clearly defined correlation between OSF density and the O/C ratio, there is an apparent correlation between the C/O ratio. This correlation is shown more clearly in Fig.16. The preliminary data obtained then suggest that the C/O ratio is critical in determining OSF nucleation and a slight increase in carbon concentration can substantially reduce defect nucleation during oxidation.

Thus, these experiments, showed that the carbon concentration in CZ-Si controls the nucleation of thermally-induced microdefects and that the oxygen reduction ratio after annealing was dependent upon initial carbon concentration. This observation is consistent with the data Fig.16, where a small increase in the initial C content and the C/O ratio produces observable reductions in OSF densities. If indeed valid, it is conceivable that the oxygen will be bound at carbon-silicon interstitial clusters relaxing lattice strain at the periphery of the cluster and reducing the likelihood of OSF nucleation. It is also possible that the carbon-oxygen bound complex will enhance the formation of SiOx precipitates. In either case, this becomes a critical point for VHSIC programs, since both C and O will have to be maintained within prescribed concentration limits.

3.5 WAFER WARPAGE AND OXYGEN CONCENTRATION

The results of earlier studies suggest that variations in oxygen concentration would be effective in enhancing wafer warpage after sequential heat cycling. To further investigate

TABLE 4. CARBON/OXYGEN CONCENTRATION RATIOS AMD AVERAGE OSF DENSITIES

Sample	Oxygen Conc. (ppm)	Carbon Conc. (ppm)	O/C	C/O	Average Defect* Density (cm^{-2})
AR010980A AR012480A AR013030C	20.3	0.41	49.5	.020	4.01×10^4
AR010980C AR012480C AR013080C	18.7	1.29	14.5	.069	1.8×10^4
AR010980D AR012480D AR013080D	17.9	1.69	10.6	.094	8.1×10^3

*After oxidation

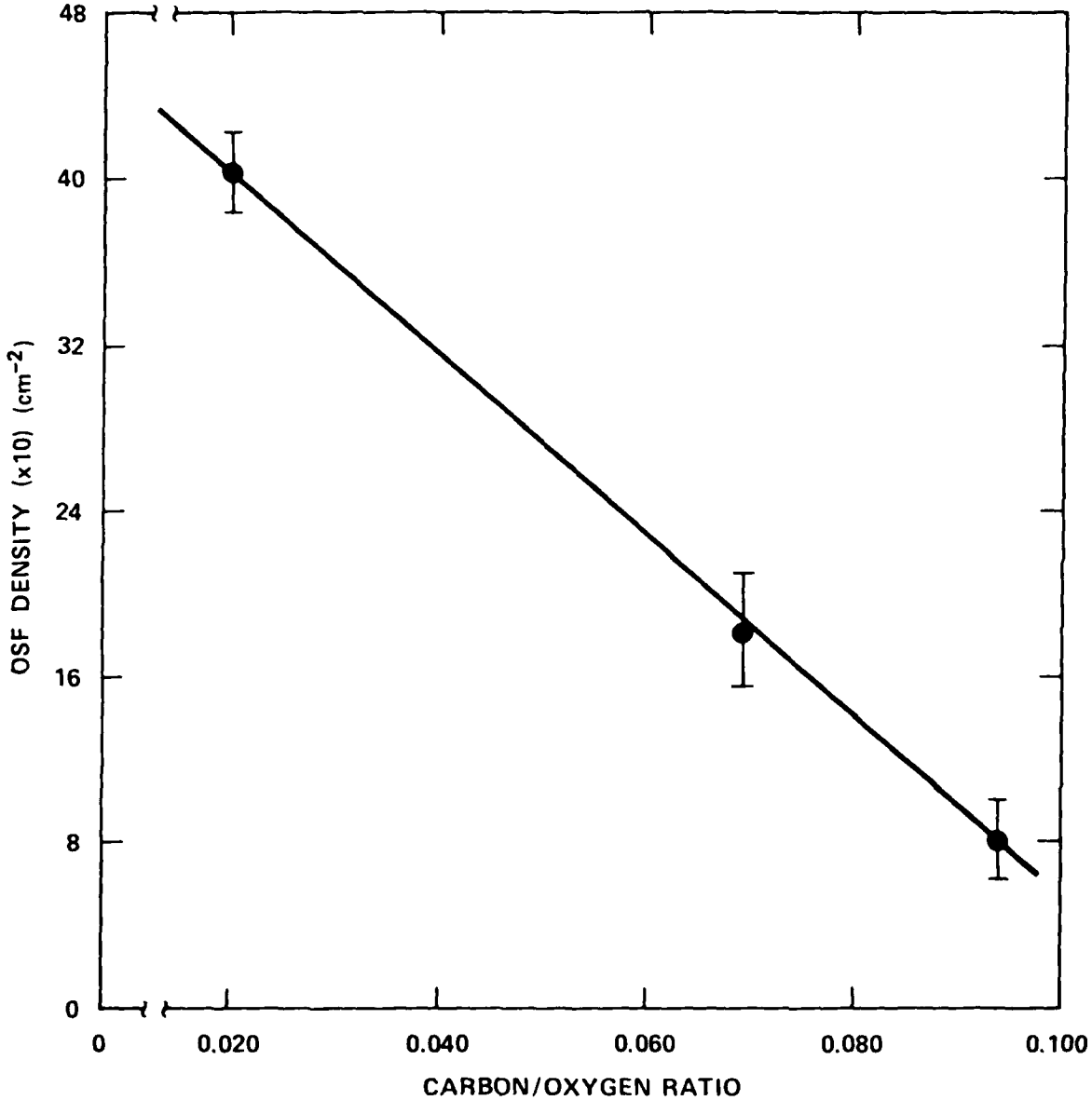

FIG. 16. OXIDATION-INDUCED STACKING FAULT DENSITY AS A FUNCTION OF CARBON/OXYGEN CONCENTRATION RATIO.

this possibility in relation to wafer quality, a series of experiments were conducted on wafers supplied by manufacturers. Infrared absorption measurements were obtained at several spots on the wafer and average oxygen concentrations determined. As stated in the Introduction, the present study is concerned with a statistical sampling; subsequently, wafers from production-line runs were used rather than optimally-prepared samples provided by a supplier.

Average oxygen concentrations, determined from FTIR measurements, were in the range, 19 to 40 ppm. Wafers were subjected to thermal cycling from 1050°C to room temperature, using withdrawal rates of 1 cm/sec and 5cm/min. After cycling, a Tropel laser interferometer was used to determine the maximum deformation or deviation between high and low positions on the wafer.

Table 5 provides a summary of data obtained on selected wafers after heat cycling. In each case, the wafers were subjected to rapid withdrawal from the furnace during cycling. In separate experiments where slow withdrawal rates were used, the maximum deformation was reduced by a factor of 2 to 3.

From the data obtained, we observe that wafers containing the highest concentration of oxygen typically exhibited the largest deformation, seemingly independent of supplier. Conversely, wafers containing smaller concentrations of oxygen generally showed the least amount of deformation. However, the lack of any consistent linear dependence of deformation on oxygen concentration also suggests that lateral variations in oxygen content play an important role in the observed warpage. An examination of the FTIR data showed that the initial oxygen concentration varied radially

TABLE 5. SUMMARY - WARPAGE TESTS ON SELECTED WAFERS CONTAINING VARIABLE OXYGEN CONCENTRATIONS

WAFER	OXYGEN (ppm)	HEAT CYCLES	WARPAGE (μm)
TI (CZ)	40	3	300
TI (CZ)	35	2	250
Monsanto (CZ)	28	3	200
NBK (CZ)	30	2	200
Shinetsu (CZ)	19	2	10
Wacker (CZ)	30	2	210
Monsanto (CZ)	21	2	60
Siltec (CZ)	30	2	150
Wacker (CZ)	35	3	300
Osaka Titanium (CZ)	21	2	30

*Warpage dependent upon both initial content and spatial variation in concentration.

**Carbon/oxygen ratio dependence not determined.

by as much as 25 to 30% on particular wafers, Hence, the deformation encountered during thermal cycling depends upon both the total oxygen concentration and the lateral distribution of oxygen within the wafer.

For comparison, we show in Fig.17 the warpage obtained by Sony Corporation investigators in Si wafers grown by the float-zone, conventional-Czochralski and magneto-Czochralski techniques.[6,7] It is of interest to note that the magneto-Czochralski (MCZ) wafer exhibits the least amount of deformation after thermal cycling. Since the MCZ technique results in lower concentrations of oxygen and uniform lateral distributions, the results appear consistent with our tests of conventional CZ grown wafers, where low oxygen levels and reduced lateral variability produced the lowest levels of deformation.

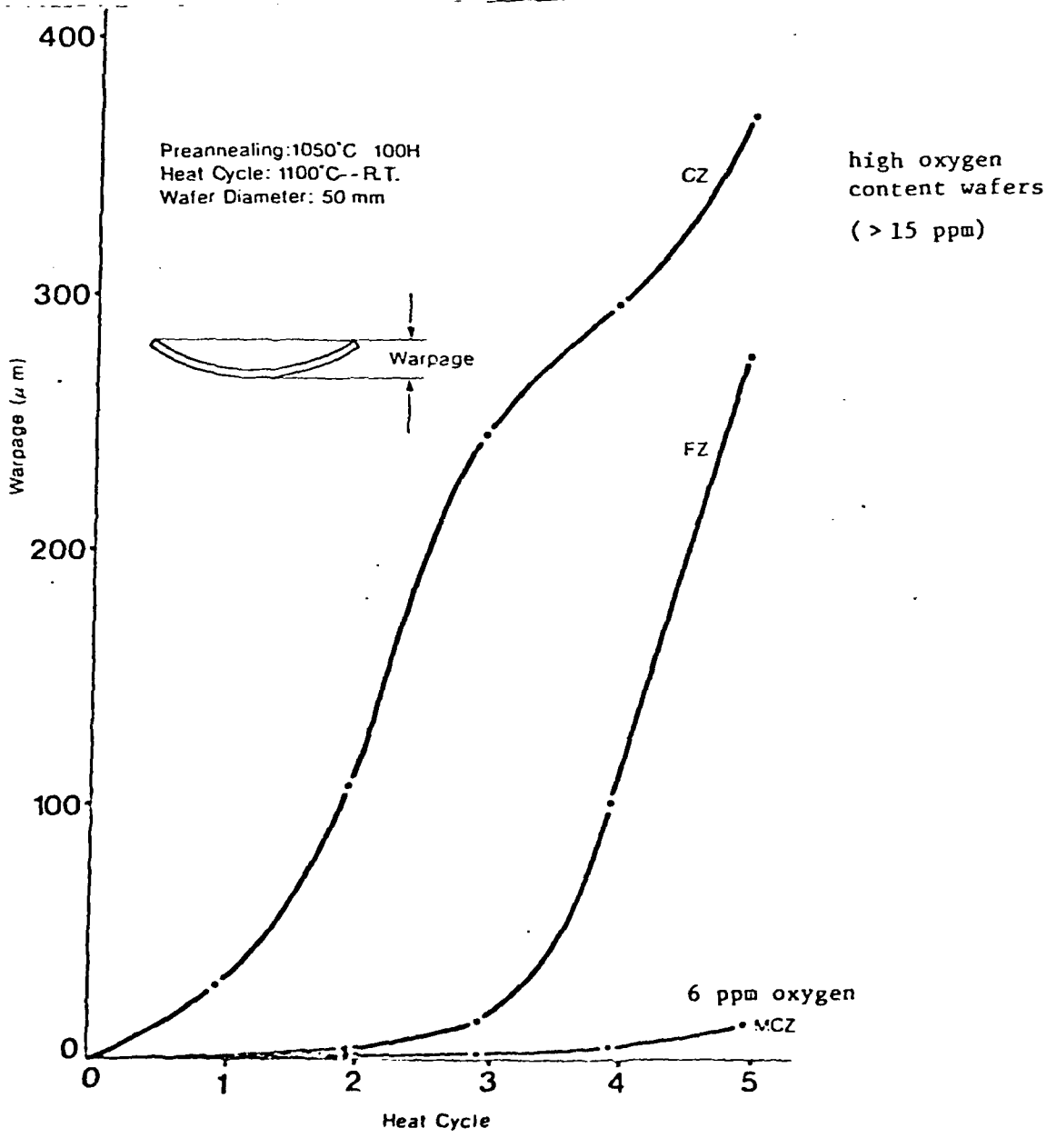

FIG. 17. PLOTS OF WAFER WARPAGE IN VARIABLE OXYGEN CONTENT CZ, MCZ AND FZ WAFERS AFTER THERMAL CYCLING (SONY CORPORATION).

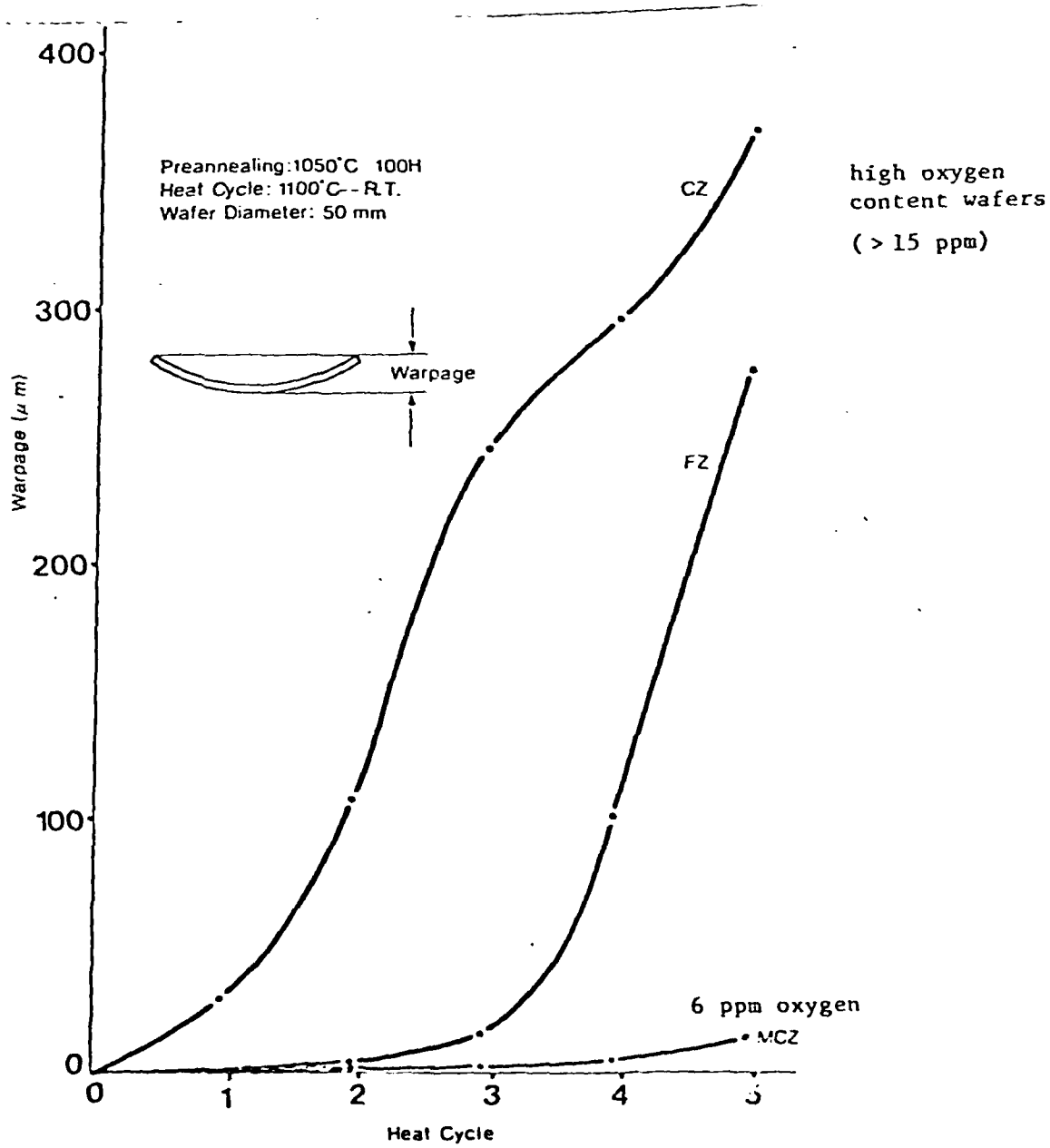

FIG. 17. PLOTS OF WAFER WARPAGE IN VARIABLE OXYGEN CONTENT CZ, MCZ AND FZ WAFERS AFTER THERMAL CYCLING (SONY CORPORATION).

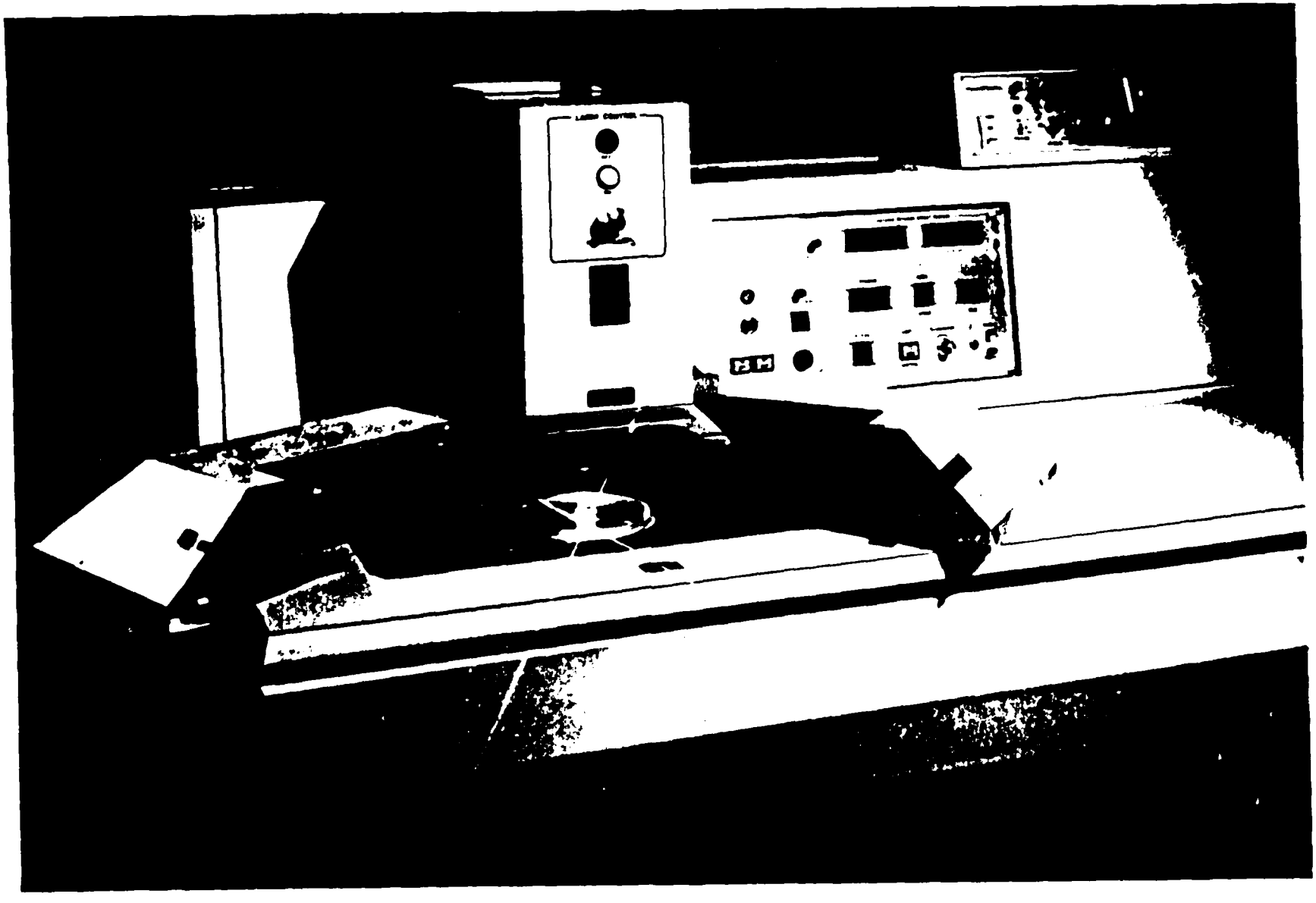

FIG. 18. ARACOR SCANNING ARGON-CW LASER ANNEALING SYSTEM.

To initially test the feasibility of laser gettering, we irradiated the front surfaces of (100) and (111) wafers at levels slightly below or within melt conditions. Fig. 19, provides optical micrographs obtained on laser-annealed (111) and (100) Si wafers after oxidation and subsequent etching of the wafer surface. In Fig. 19a), we observe that defects are prominently displayed along the laser scan lines on the (111) wafer surface, with the regions adjacent to scan lines exhibiting an apparent absence of defects. In Fig.19b) for the (100) wafer, we observe a similar pattern of defect denudation adjacent to laser scan lines. To the right of the figure, we note that OSF etch figures are present within the control (unirradiated) section of the wafer. Effective elimination or reduction of OSF densities occurs to distances >250 μm from the edge of the laser scan line.

Since the strain field produced by the laser-induced defects can be assumed to be radially symmetric, we can assume that interaction distance for gettering of defects and OSF nucleation sites is also greater than 250 μm. From these results, we can assume that laser irradiation of the back surfaces of wafers would be effective in gettering of defects at the front surfaces of wafers, since the range of the interaction field generally exceeds the thickness of wafers used in processing.

To further investigate the use of back-surface laser gettering, we irradiated samples at powers approximately at the level required to produce melting, using line separations of 75 μm (edge to edge). In these experiments, one-half of each wafer was subjected to laser annealing and the other half served as a control section. After laser annealing, the wafers were subjected to wet oxidations at 1100°C. After stripping the oxide layers, the wafers were immersed in a modified Secco solution to expose OSF at the front surface.

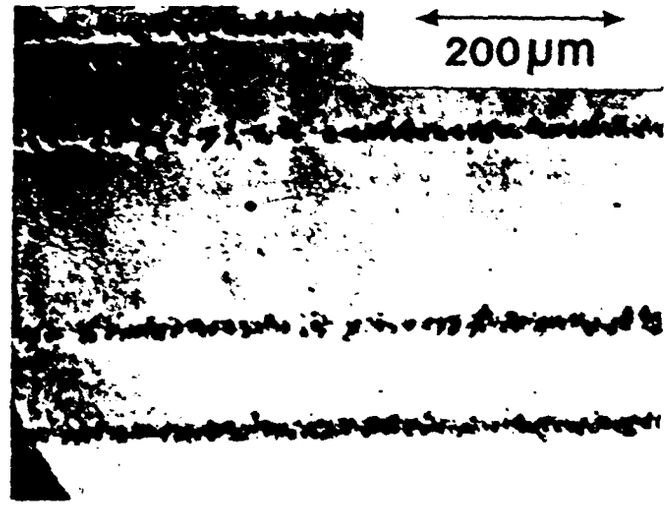

(a)

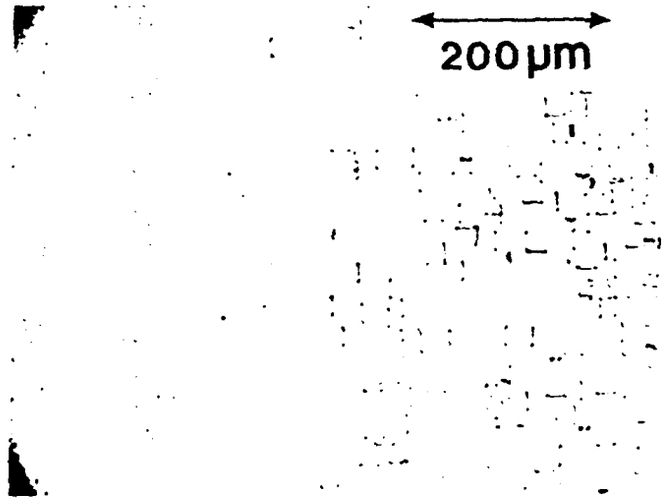

(b)

FIG. 19. OXIDATION-INDUCED STACKING FAULTS AT THE FRONT SURFACES OF SILICON WAFERS SUBJECTED TO (MELT-SUBMELT) LASER ANNEALING ON FRONT SURFACES; a) (111) Si WAFER-DEFECTS SHOWN GETTERED ALONG LASER SCAN LINES; b) (100) Si WAFER-CONTROL SECTION-RIGHT, LASER SCANS TO LEFT.

In Figure 20 shows optical micrographs obtained at the front surfaces of back-surface laser-annealed samples. In both cases, we observe that the regions corresponding to the gettered sides exhibit significant annihilation of OSF defects, while in the control sections, OSF densities remain high.

To further evaluate the effect of laser irradiation conditions, we conducted a series of experiments in which the laser lines were overlapped (40%) and separated by variable distances. When overlapping lines were utilized, we found that the gettering efficiency was reduced. Subsequent TEM evaluation showed that when overlapping lines were utilized, the defect structure induced at the edge of the first laser line was partially annihilated during the second overlapping line scan, thereby reducing the net back-surface defect concentration and the strength of the strain field responsible for gettering. In a series of experiments, we found that edge-to-edge line separations of $\simeq$ (0.75) d_B, (d_B = laser focal spot diameter), were optimal for our irradiation conditions.

To determine the effectiveness or relative laser gettering efficiency, a series of wafers was subjected to back-surface laser irradiation under identical conditions except for variations in the laser power. After laser-irradiation, standard oxidation and etch procedures were used and the etch figures measured for control (no laser irradiation) and laser irradiated wafers. To provide a measure of the relative gettering efficiency, we used the ratio of etch-figure concentration in control, D_{NL}, to concentration within the laser-scanned region, D_L, to define the relative gettering efficiency, α, where $\alpha = D_{NL}/D_L$.

Figure 21 shows a plot of α vs. laser power. We observe at laser powers <12W, that the efficiency is <1, implying a

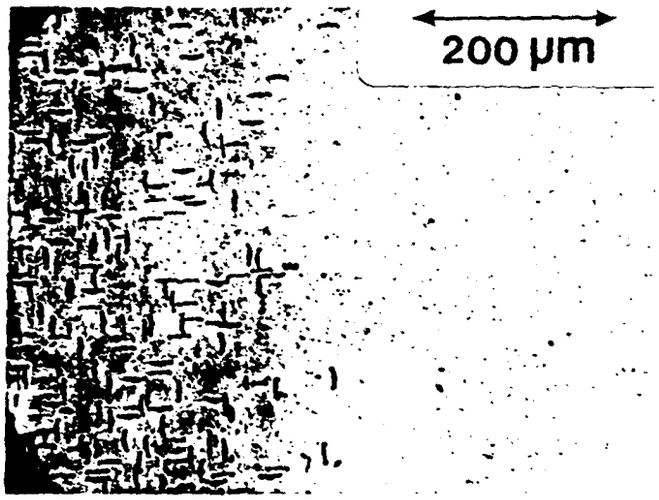

(a)

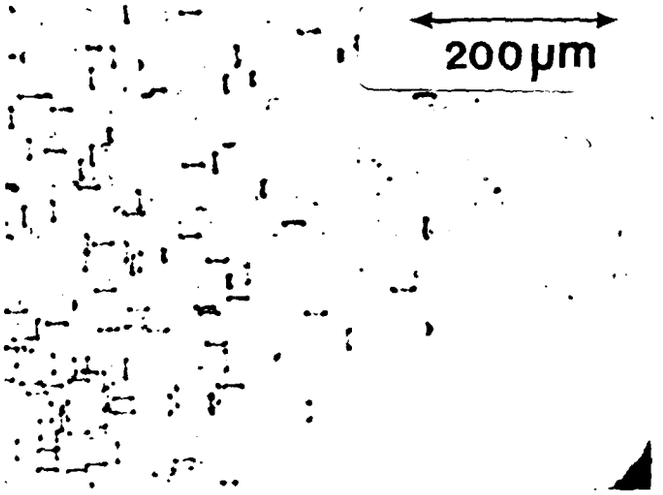

(b)

FIG. 20. OXIDATION-INDUCED STACKING FAULTS AT THE FRONT SURFACES OF SILICON WAFERS SUBJECTED TO BACK-SURFACE LASER GETTERING.

$$\text{RELATIVE LASER GETTERING EFFICIENCY} = \frac{D_{NL}}{D_L} = \frac{N_i}{N_i^*}$$

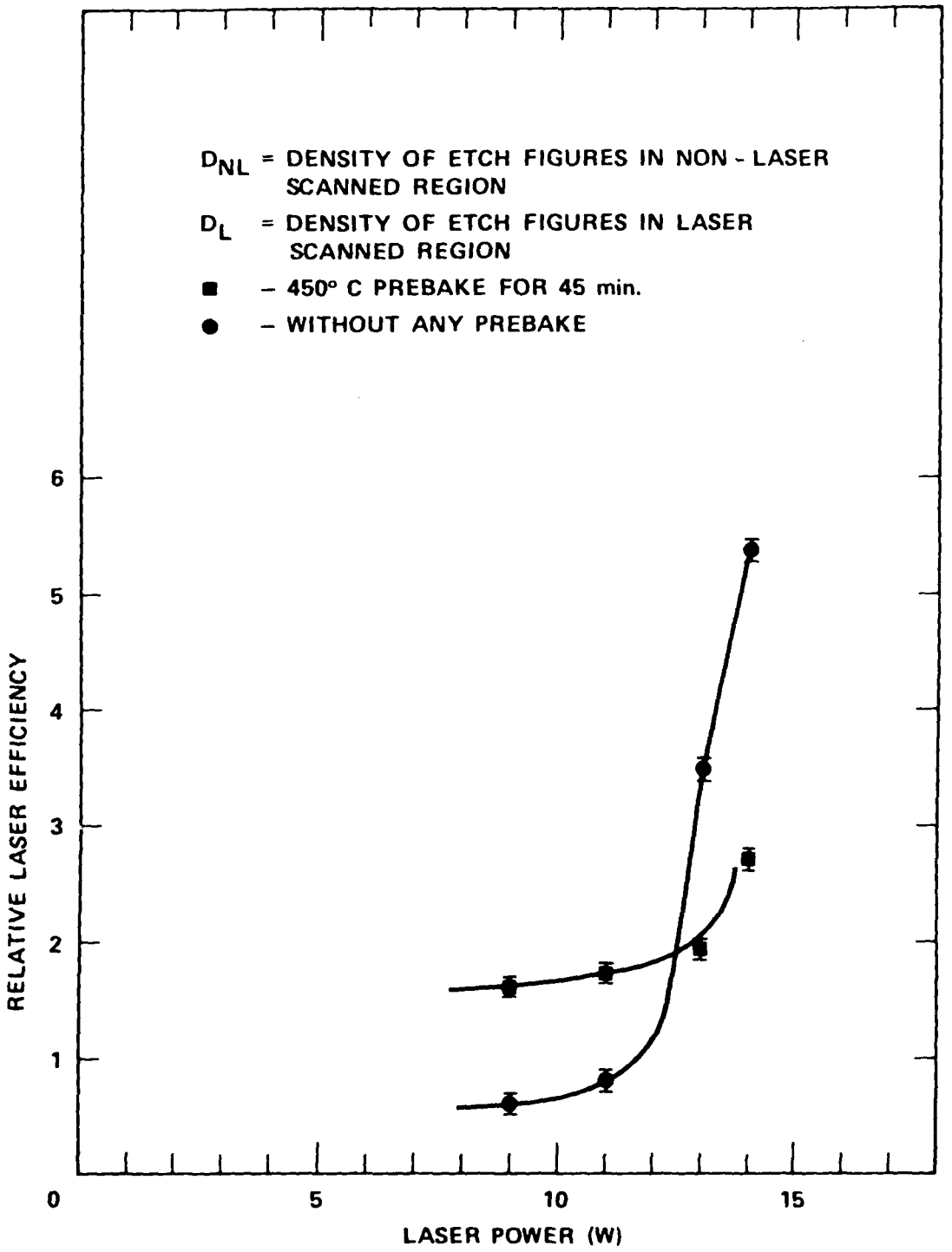

FIG. 21. PLOT OF RELATIVE (BACK-SURFACE IRRADIATION) LASER GETTERING EFFICIENCY AS A FUNCTION OF LASER POWER; OSF DENSITITES MEASURED AT FRONT SURFACES.

creation of defects or increase in OSF density. Conversely, in the submelt region (12W <P $\leq$13W), the efficiency is dramatically increased, producing an OSF annihilation factor of $\simeq$ 80%. At laser powers > 13W, well within the melt regime, we observe no further increases in gettering efficiency, and α remains at $\simeq$ 5.5. For wafers irradiated at power levels < 12W, we observed that a 450°C post-laser, pre-oxidation anneal produced an increase in the gettering efficiency (Fig. 21).

Our initial data did not permit a reasonable explanation for this increase in gettering efficiency after post-laser thermal annealing. However, subsequent experiments, in which low temperature anneals were shown to produce damage stabilization (Section 4.3), provide some insight onto the results obtained in these experiments. Partial stabilization of laser-induced damage is attained under the conditions utilized, although the conditions are not optimal for complete stabilization. Upon subsequent oxidation, the (partially) stabilized damage will prove effective in gettering of point defects responsible for OSF nucleation, thereby producing an effective increase in relative gettering efficiency.

4.2 FRONT-SURFACE LASER GETTERING OF WAFERS FOR VHSIC APPLICATIONS

In the previous section, we discussed the application of back-surface laser irradiation for gettering of impurities and defects in bulk Si wafers. In this section, we will discuss the use of front-surface gettering procedures for the gettering of defects and impurities in zones nearest to processing regions.

In these experiments, we used scanning Ar laser irradiation of wafers maintained at room temperature. Separate

tests were also conducted using substrate temperatures of 150°C. A scan line overlap factor of 30 to 40% and a scan velocity of $\sim$ 10 cm/sec was used during laser irradiation. The focal spot size was 50 μm and laser powers were varied between 3W and 9W.

To provide control data,we irradiated half of each wafer and retained the remaining section for comparative analysis. Subsequent to laser irradiation, wafers were cleaned and subsequently (wet) oxidized at 1100°C for 3 hrs. After removing the oxide layers, both control and laser-annealed samples were immersed in a modified Secco etching solution to expose defects and OSFs at the wafer surfaces.

In Figure 22 shows representative optical micrographs obtained within the control section (no laser pre-treatment). (Fig. 22a) and laser irradiated section of a wafer. We observe that the density of OSF etch figures is considerably reduced in the section exposed to laser irradiation. A histogram plot of the number of etch figures, as a function of position along a diameter of the wafer, is shown in Fig. 23. Relative to the control section, a reduction in OSF density $\sim$ 80% is observed.

To determine the depth of effective gettering, a series of samples were subjected to sequential oxidations and subsequent Secco etches. For equivalent depths <3 μm, we observed a similar pattern of OSF distribution with densities substantially reduced within the laser pre-treated sections. At depths >3 μm, however, no variation in OSF densities were detected within laser-irradiated or control sections, suggesting that the range of gettering under these conditions is <3 μm. These tests were repeated on a number of wafers with essentially identical results. For some of the worst wafers identified in this study, we were able to achieve substantial reductions in oxidation-induced defects.

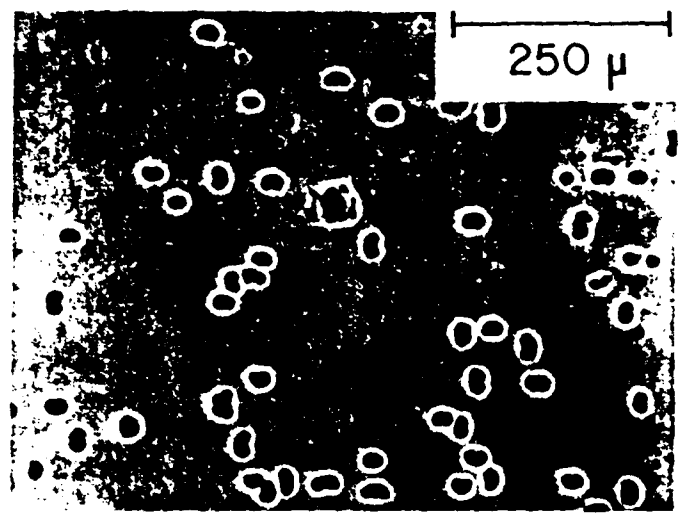

(a)

(b)

FIG. 22. OPTICAL MICROGRAPHS OF (100) SILICON WAFER AFTER LOW-POWER, FRONT-SURFACE LASER IRRADIATION, OXIDATION AND ETCHING; a) CONTROL; b) LASER IRRADIATED.

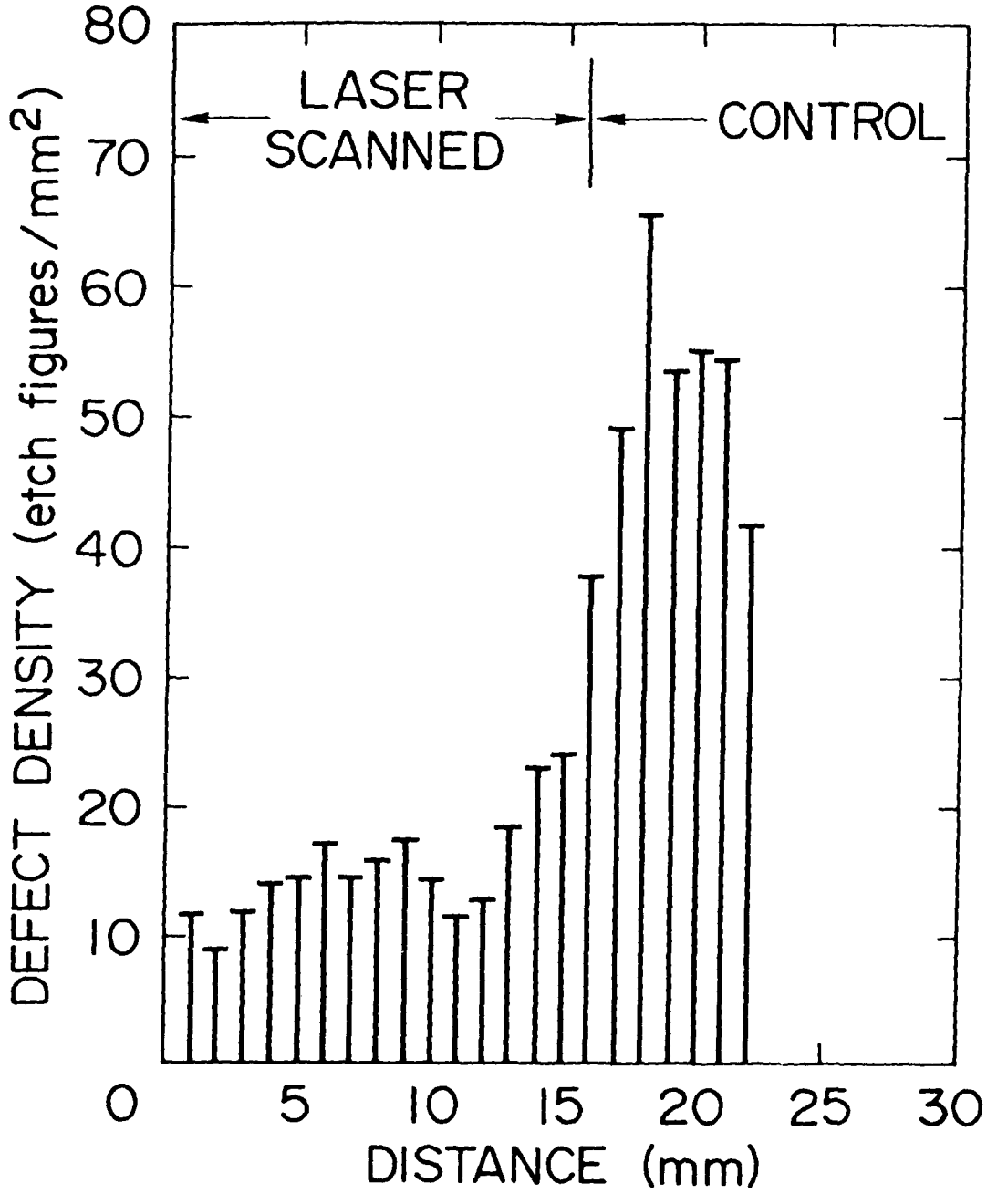

FIG. 23. HISTOGRAM PLOT OF DEFECT DENSITIES (FRONT SURFACE) AFTER 1100°C WET OXIDATION OF FRONT-SURFACE LASER-GETTERED WAFERS WITHIN BOTH CONTROL (NO LASER IRRADIATION) AND LASER SCANNED REGION.

Under the conditions used in this study, $P<<P_{melt}$ and melt-resolidification induced defects are not present. In like manner, slip lines are also not generated. However, quenched-in point defects and clusters are introduced at depths >1 μm, as confirmed in DLTS measurements at Xerox Research Laboratories and Bell Laboratories, and by direct TEM observation at ARACOR. These cluster zones provide the gettering sites for fast-diffusing metallic impurities and defects that serve as nucleation regions for OSF formation.

From the results obtained, the technique appears advantageous for application to VHSIC processing, since it can be readily used either singly or in conjunction with other bulk gettering techniques. Of extreme importance, however, is the fact that effective gettering is produced directly at the front surface.

4.3 BACK-SURFACE DAMAGE STABILIZATION FOR INCREASED GETTERING EFFICIENCY

The use of various gettering techniques has been an accepted procedure in Si processing for the past 20 years. In each case, however, there are particular disadvantages inherent in its application. One common factor is the lack of thermal stability over long, high-temperature annealings, as would be typically encountered during processing. Damage introduced into the back surface of a wafer by ion implantation, diffusion, or mechanical abrasion is largely annealed after 45 minutes of annealing at 1000°C, reducing the gettering efficiency and producing "reverse" gettering or the release of trapped impurities that diffuse back into the interior of the wafer. The use of intrinsic gettering or internal SiOx precipitation is also unstable at temperatures exceeding 1100°C. At temperatures in the 1100 to 1200°C range, dissolution of the SiOx precipitates occurs, resulting in the annihilation of internal gettering sites.

To further investigate the problem of thermal stability, we began a series of experiments on double-phase annealing of back-surface, mechanically-damaged wafers to determine if the annealing behavior could be altered. As a result of these studies, we have identified a technique and investigated mechanisms for stabilization of back-surface damage in gettering regions. In addition, we have now shown the enhanced diffusion of oxygen in the presence of defects in Si wafers.

Samples used in this study were n- and p-type, 75-mm diameter, 400-μm thick CZ-Si wafers of [100] orientation ($\pm 1°$). Oxygen concentrations in the range, 1.0 to 1.2 x 10^{18} cm^{-3}, were determined by Fourier transform infrared (FTIR) absorption measurements on unannealed wafers using ASTM procedures[1]. Back-surface damage was introduced in Si wafers using a rotary abrasion technique [8-9] to create concentric spiral grooves extending to an average depth of $\simeq$ 8 to 10 μm into the surface. Annealing was done either in a flowing N_2 atmosphere or in an oil-free vacuum system at a vacuum level of $\simeq$ 10^{-8} Torr. In separate experiments, samples were annealed under the following conditions: a) 600°C, 1 to 24 hours, b) 1050°C, 1 to 15 hours, c) 600°C, 24 hours + 1050°C, 1 to 15 hours and d) 1050°C, 1 to 5 hours + 600°C, 1 to 10 hours.

Specimens for TEM analyses were prepared by a modified jet thinning procedure. Horizontal sections were prepared by first immersing in a calibrated (9:1) HNO_3: HF etch solution to remove material within damaged regions and subsequently jet thinning from the front surface. Vertical-cross-section samples were prepared from a series of stacked 800-μm x 3000-μm strips cut along a <110> direction and embedded in epoxy resin (EPON-812). After chemical/mechanical polishing to a thickness of 150 μm, specimens were ion milled in a Commonwealth Scientific instrument.

Secondary ion mass spectrometry was used to obtain oxygen impurity profiles at the back surfaces of the Si. Samples for cross-sectional SIMS imaging[10] were cleaved along a <110> direction, embedded in a low melting point Sn-Bi alloy, and subjected to chemical/mechanical polishing. In all cases, specimens were analyzed in a Cameca IMS-3f microanalyzer using Cs^+ ion bombardment while detecting $^{16}O^-$ and $^{30}Si^-$ secondary ions. The oxygen concentration levels were determined using standards prepared by ion implanting oxygen into CZ-Si. Residual pressure within the sample chamber during SIMS profiling was $\simeq$ 1 x 10^{-9} Torr while sputtering at a rate of 350 Å/sec.

Transmission electron microscopic examination showed that the rotary abrasion process produced a laterally discontinuous array of nested dislocations decreasing in density as a function of depth beneath the level of macroscopic damage grooves. Annealing at 600°C for 1 to 24 hours in either vacuum or flowing N_2 produced no significant annihilation of dislocation line structure. However, dark-field electron micrographs showed the presence of small (< 250Å image diameter) microprecipitates within back-surface-damage regions, either pinned along dislocation lines or in adjacent regions, increasing in density as a function of increasing annealing duration. Examination of double-annealed (600°, 24 hour + 1050°C, 1-3 hour) samples showed a dramatic increase in dislocation line concentration (Fig. 24a) and a subsequent increase in the effective width of the damage region at the back surface. In addition, we observed the appearance of well-defined SiOx precipitates along dislocation lines and precipitate-dislocation complexes (PDC) associated with the nucleation of clustered precipitates (Fig. 24b)).

Figure 25 shows the measured dislocation line as a function of depth beneath damage grooves. In the damaged control samples and in samples annealed at 600°C for 24 hours, we

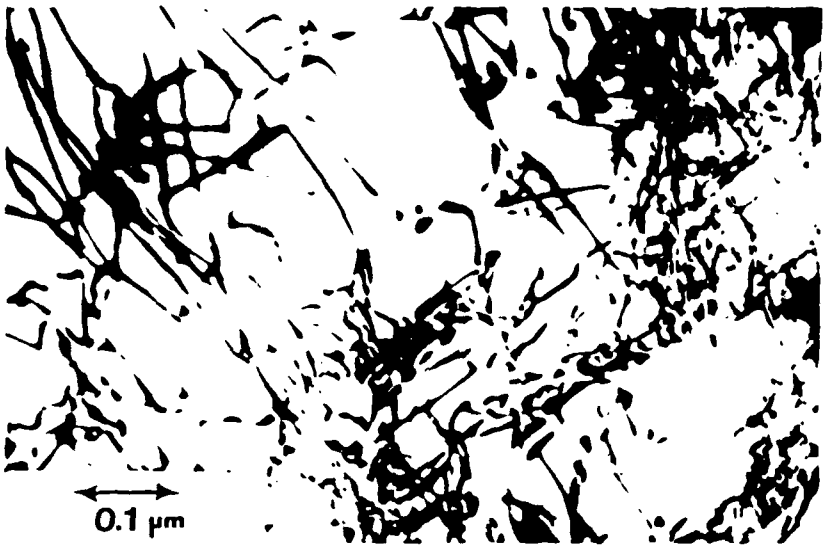

(a)

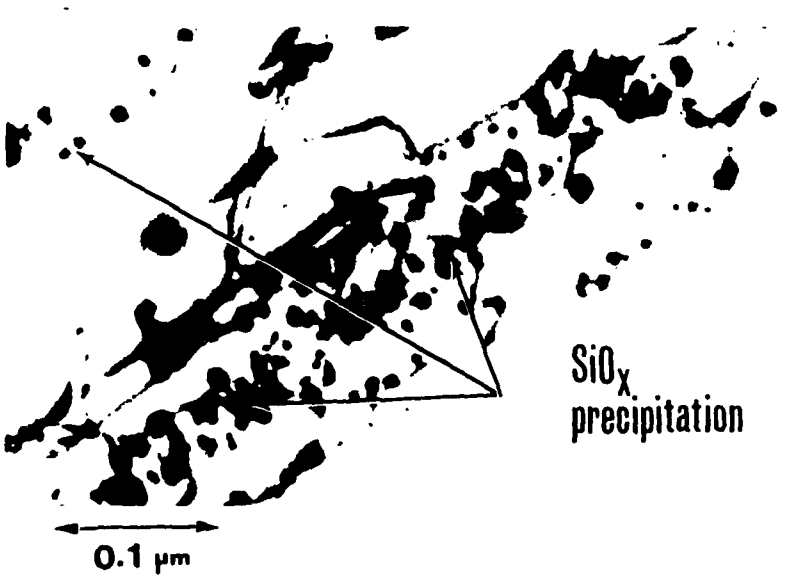

(b)

FIG. 24 BRIGHT-FIELD TRANSMISSION ELECTRON MICROGRAPHS OBTAINED ON BACK-SURFACE DAMAGED SAMPLES SUBJECTED TO VACUUM ANNEALING AT 600°C, 24 HRS. + 1050°C. 3 HR: (a) HORIZONTAL SECTION AT DEPTH OF ~ 5 μm BELOW THE DEPTH OF DAMAGE GROOVES: (b) HIGH MAGNIFICATION MICROGRAPH SHOWING THE PRESENCE OF DISLOCATION LINES NUCLEATED WITHIN CLUSTERED SiOx REGIONS.

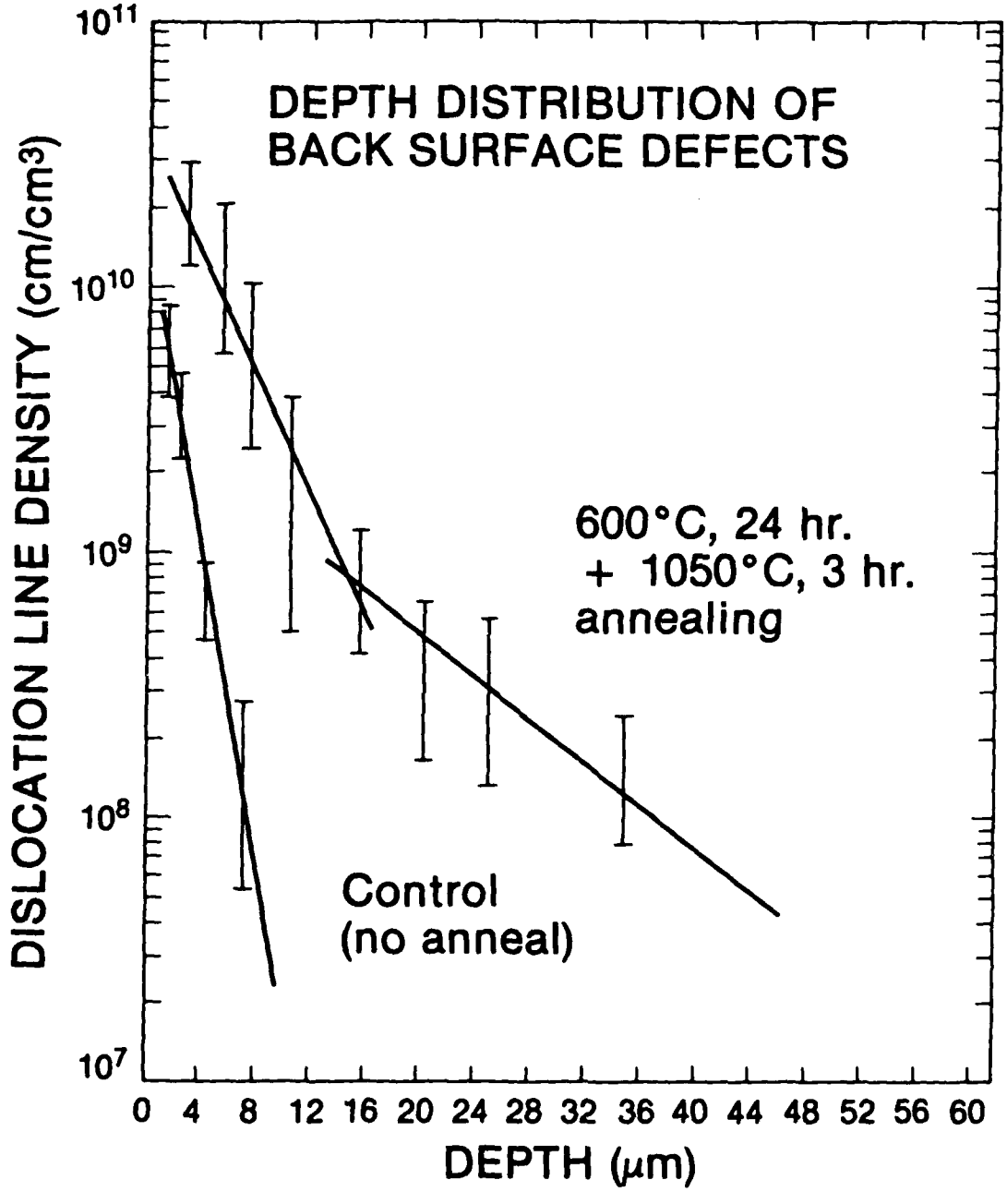

FIG. 25. DISLOCATION LINE DENSITY AS A FUNCTION OF DEPTH FOR CONTROL AND DOUBLE-ANNEALED SAMPLES.

observed a vertically-graded dislocation line structure extending to an estimated depth of $\sim$ 10 μm. After double annealing in either vacuum or flowing N_2, we observed a significant increase in the dislocation line density within the near-surface (< 10 μm) region and a zone of secondary line structure extending to a depth $\leq$ 40 μm.

To provide further information on the depth distribution of primary and secondary damage, vertical-cross-section samples were prepared for TEM analysis. Damaged (unannealed) and 600°C annealed samples contained dislocation lines extending to a depth $\sim$ 10 μm, in agreement with horizontal sectioning measurements. Examination of double annealed (600°C + 1050°C) samples ([110] surface) showed a heavy concentration of dislocation lines and precipitates within a near-surface region (depth $\leq$ 14 μm) and a secondary zone of dislocation lines extending from the periphery of the region to a depth of $\sim$ 40 μm. Figure 26 is a representative (vertical cross section) electron micrograph obtained at the edge region of the two zones, (d $\leq$ 14 μm) showing the development of secondary microstructure and precipitation within the primary damage region.

Horizontal sectioning measurements show that $\sim$ 80% of the dislocation line structure is annihilated after a 3-hour, 1050°C anneal. If this high-temperature step is followed by 600°C annealing, the development of secondary dislocation line structure (Fig. 26) is not observed.

A correlation between dislocation line structure and oxygen redistribution was obtained from SIMS profiles of the oxygen concentration beneath damage grooves. Figure 27 shows the SIMS oxygen profiles in control (unannealed) and annealed samples. The control sample shows essentially no redistribution of oxygen, whereas annealing at 1050°C for 1 to 3 hrs. causes

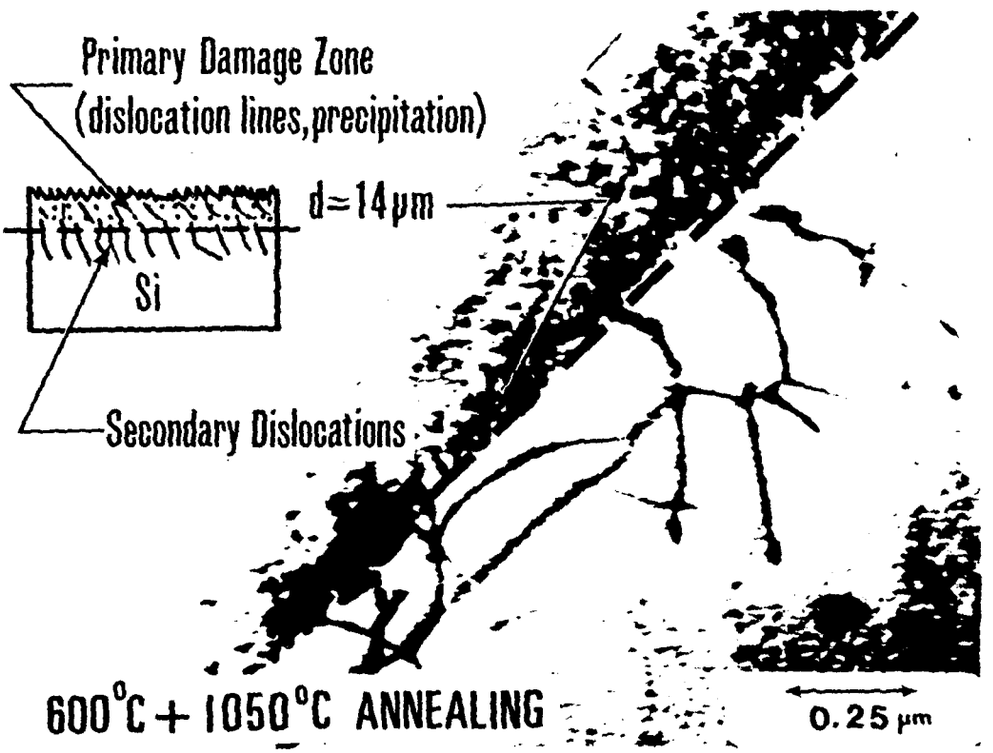

FIG. 26. BRIGHT-FIELD ELECTRON MICROGRAPHS OBTAINED ON VERTICAL-CROSS-SECTION SAMPLES ({[100]PLANE) AT DEPTH OF ~ 14 μm AFTER ANNEALING AT 600°C FOR 24 HRS. FOLLOWED BY A 3-HR ANNEAL AT 1050°C.

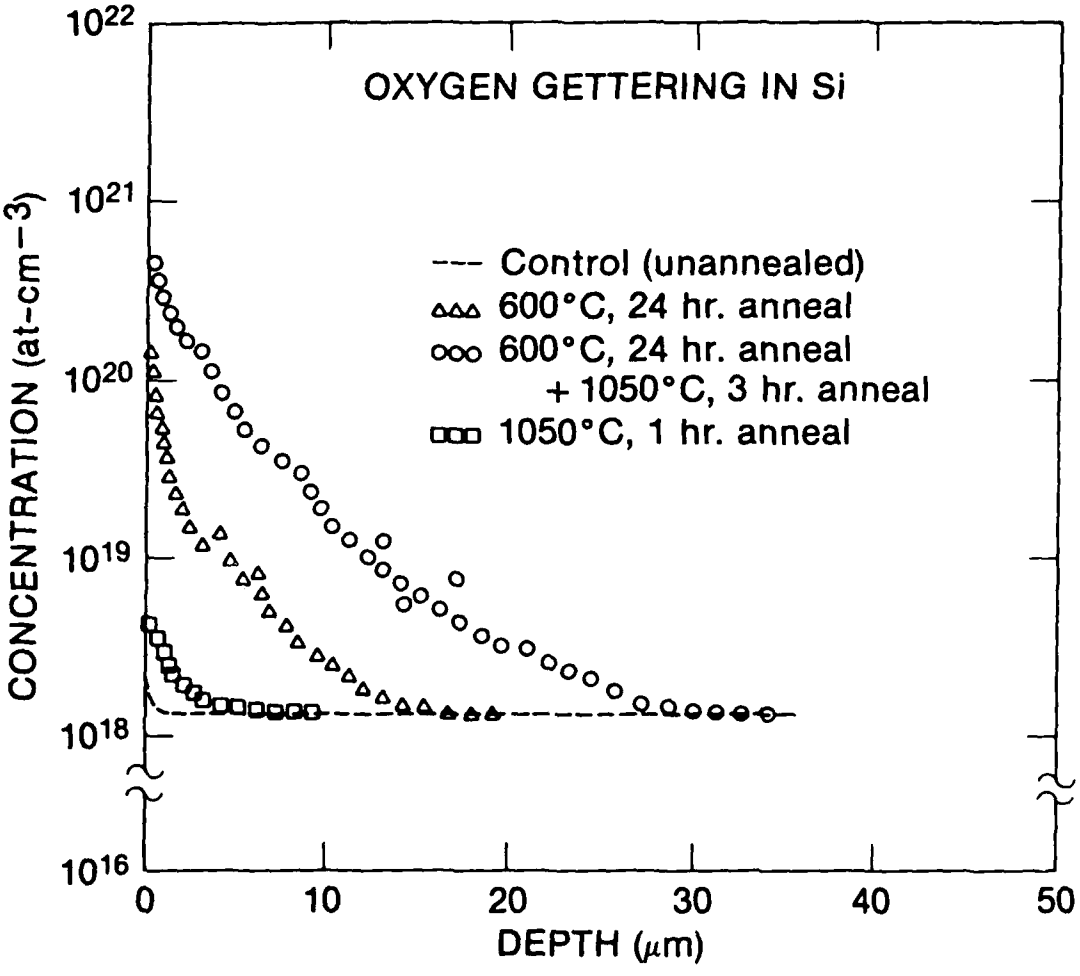

FIG. 27. SIMS PROFILES OF OXYGEN CONCENTRATION AT BACK-SURFACE OF DAMAGED, ANNEALED SAMPLES.

oxygen redistribution. Annealing at 600°C for 24 hours produces substantial motion and gettering of oxygen into back-surface-damage regions. Comparing Figs. 25 and 27, we observe that the oxygen is gettered within a region corresponding to the near-surface dislocations. Correspondingly, when the low-temperature annealing is followed by a 3-hr., 1050°C annealing treatment, the oxygen profiles again closely parallel the dislocation line density distribution shown in Fig. 25.

Ion micrographs (Fig.28) obtained on vertical cross-sections of annealed samples provide further supportive data on the correlation between oxygen redistribution and damage structure. After annealing at 600°C, dislocation lines are decorated with oxygen atoms and extend to a depth of $\simeq$ 10 μm. After subsequent annealing at 1050°C, the oxygen concentration is dramatically increased within the near-surface region, producing a band of precipitated oxygen (Fig. 28b)). Secondary dislocation lines decorated with oxygen extend from the edge of the primary damage zone to a depth of $\simeq$40 μm. We detected no internal oxygen banding or secondary damage structure with correlated oxygen precipitation in undamaged or 1050°C annealed samples.

From these data, we conclude that annealing of back-surface-damaged samples at 600°C produces rapid redistribution and gettering of mobile oxygen along dislocation lines. This primary damage is stabilized or pinned in the presence of oxygen,[11] with negligible annihilation upon further annealing at 600°C. Subsequent annealing at 1050°C produces additional gettering, oxygen precipitation and an increase in dislocation line density, both within PDC clusters and as a result of increased strain fields created by the excessive SiO_x precipitation. Secondary dislocation lines extending to a depth of $\geq$ 40 μm are thought to be generated by large strain fields associated with misfit between

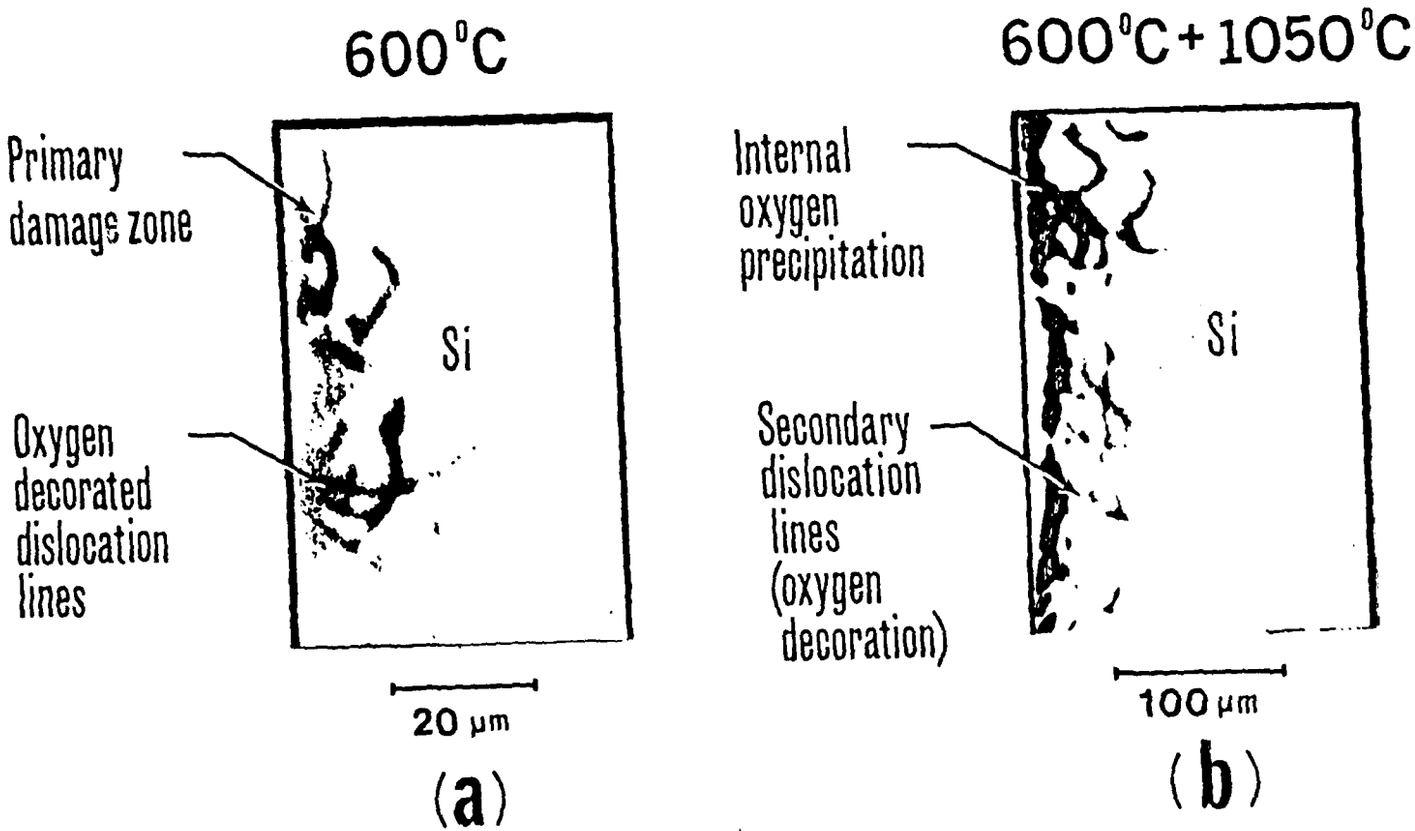

FIG. 28. SECONDARY ION MICROGRAPHS SHOWING OXYGEN IMAGES OBTAINED ON {110} PLANES WITHIN BACK SURFACE DAMAGE REGIONS OF WAFERS SUBJECTED TO ANNEALING; A) 600°C, 24 HRS; B) 600°C, 24 HRS. + 1050°C, 3 HRS.

SiOx precipitates and the Si lattice within a heavily precipitated near-surface region. After forming, the secondary dislocation lines serve as sinks for additional gettering of oxygen.

In additional tests, we found that the damage at the back-surface was stable and did not suffer annihilation after extended 15-to 30-hr. anneals at 1100°C. These results demonstrate that gettering is stabilized and persists throughout a processing sequence.

In an earlier section (4.1), we discussed the use of back-surface laser irradiation for gettering applications. In the experiments conducted, preliminary data indicated that a low temperature primary anneal after laser exposure would tend to stabilize damage and increase the gettering efficiency. The present data now clearly begin to define the procedures that will be effective for stabilization of laser gettering.

4.4 LOW-TEMPERATURE REDISTRIBUTION AND GETTERING OF OXYGEN IN SILICON

In a recent paper,[12] it was shown that oxygen could be readily gettered from the interior into back-surface-damage regions of Czochralski (CZ) Si wafers after annealing at temperatures in the range, 600° to 1050°C. Because of the relative importance of the subject of oxygen redistribution in Si, it is essential that the motion of oxygen in bulk Si be properly assessed and understood. To extend the results of the initial investigation on the rapid redistribution of oxygen, a series of experiments were conducted using transmission electron microscopy (TEM), secondary ion mass spectrometry (SIMS) depth profiling and secondary ion microscopy to determine if oxygen can be gettered at temperatures in the range, 300° to 500°C.

Samples for these experiments were n- and p- type, 75-mm diameter, 400 μm thick CZ-Si wafers of [100] orientation. Oxygen and carbon concentrations of 1.0 to 1.1 x 10^{18} cm^{-3} and 1.9 x $10^{16}cm^{-3}$, respectively, were determined by Fourier transform infrared (FTIR) absorption measurements on unannealed wafers using ASTM procedures[1]. Rotary abrasion techniques[8,9,12] were used to create concentric grooves of 8-to 10- μm depth into the back surfaces of wafers. Annealing was done in either flowing Ar or in an oil-free vacuum system at a pressure of $\sim 10^{-8}$Torr. Samples were annealed in separate experiments at temperatures between 300° and 500°C for periods of 10 to 72 hours.

Control and annealed samples were prepared for TEM analysis in the form of 3-mm x 3-mm parallelopipeds. Conventional jet thinning techniques were used to produce electron transparent regions (<3500 A thick) for examination in the electron microscope. Horizontal sectioning[12] was used to obtain a quantitative measurement of the distribution of microstructural damage as a function of depth at the back surface of damaged wafers.

Oxygen concentrations at the back surfaces of control and damaged, annealed samples were determined using SIMS depth profiling. For cross-sectional analysis, samples were cleaved along a <110> direction, and cut into 1-mm x 5-mm strips. The strips were subsequently stacked and embedded in a low-melting-point Sn-Bi eutectic alloy. After chemical/mechanical polishing, the specimens were introduced into the chamber of the mass spectrometer and lateral oxygen distributions obtained in the ion imaging mode of operation[10]. All samples were analyzed in a Cameca IMS-3f microanalyzer using Cs^+ primary ion bombardment while detecting $^{16}O^-$ and $^{30}Si^-$ secondary ions. Calibration standards for determining oxygen concentrations were prepared by ion implantation of ^{16}O into CZ-Si.

Examination by TEM of control (undamaged) and back-surface-damaged (unannealed) samples showed that a laterally-discontinous complex network of dislocation nests and tangles, extending to a depth of >10 μm, was produced by the rotary abrasion process. The dislocation density was observed to decrease as a function of depth, resulting in a vertically-graded defect distribution at the back surface of the Si wafer. After annealing at temperatures in the range, 300° to 500°C, for periods of up to 72 hours, we observed no significant alterations in either the lateral or vertical distribution of defects within damaged regions. Careful examination of samples annealed at 300°C for 48 hours showed the presence of small microprecipitates ($\sim$100 to 150 Å average image diameter) concentrated at the edges of dislocation lines. Increasing either the annealing time or temperature produced a corresponding increase in the density of microprecipitates, accompanied by only a small increase in average image diameter.

Figure 29a) shows a representative bright-field electron micrograph obtained from the back surface of a sample after annealing at 400°C for 72 hrs. in flowing Ar. The presence of precipitates is clearly noted and observed throughout the damage region. Figure 29b) shows a schematic of the vertical cross section ([110] plane) and oxygen ion micrograph obtained from a sample annealed at 400°C for 72 hrs. in flowing Ar. The presence of oxygen along dislocation lines at the back surface is readily observed in the secondary ion micrograph. The majority of oxygen-decorated dislocation line structure is confined to a depth of < 10 μm, beneath damage grooves at the back surface, in agreement with horizontal depth sectioning/TEM determinations of dislocation density profiles. In contrast, examination of damaged, unannealed samples in vertical cross section show no oxygen-decorated dislocation line structures by TEM and an apparent absence of any imageable oxygen (by SIMS) within damage regions at the back surface.

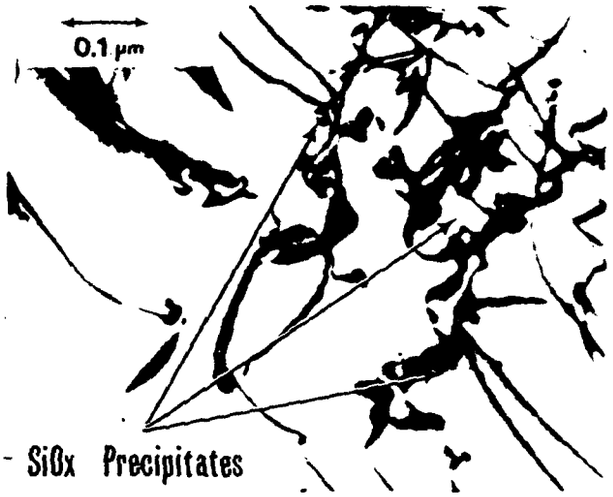

(a)

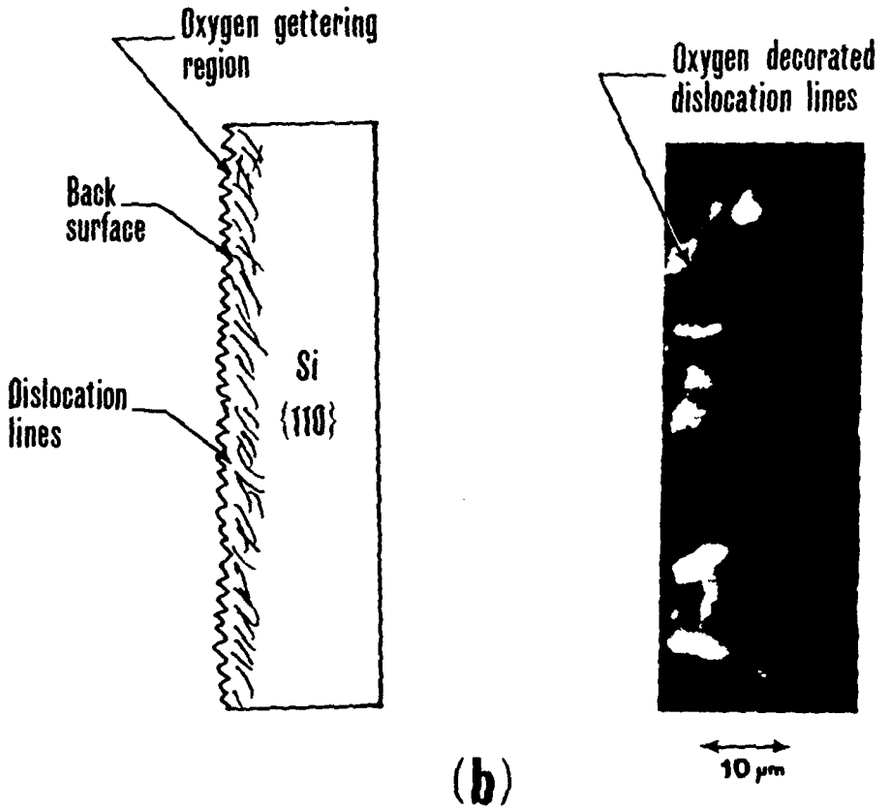

(b)

FIG. 29. BRIGHT FIELD TRANSMISSION ELECTRON MICROGRAPH AND SECONDARY ION MICROGRAPH FROM BACK SURFACE DAMAGED SILICON SAMPLE AFTER ANNEALING AT 400°C FOR 72 HOURS; A) BRIGHT FIELD ELECTRON MICROGRAPH SHOWING THE PRESENCE OF SiOx PRECIPITATES CONCENTRATED ALONG DISLOCATION LINES; B) SECONDARY ION MICROGRAPH AND SCHEMATIC SHOWING CROSS SECTIONAL SAMPLE ({110} PLANE) AND OXYGEN DECORATION ALONG DISLOCATION LINES WITHIN BACK SURFACE DAMAGE REGION.

To obtain additonal information on the redistribution of oxygen as a function of annealing temperature and annealing time, SIMS profiles of oxygen concentration as a function of depth were obtained beneath damage grooves at the back surface. Samples were annealed at 300°,350°,400° and 500°C for periods of 10 to 72 hrs. in separate experiments. For comparative purposes, we conducted identical annealing experiments in flowing Ar and under high vacuum. Annealing at 300°C for periods <24 hrs. produced no detectable gettering of oxygen within damage regions. However, for annealing times >24 hrs. (at 300°C), we were able to clearly detect the presence of gettered oxygen at the back surface. Similarly, for annealing temperatures >300°C, the redistribution and gettering of mobile oxygen was noted within damage regions and observed to increase as a function of increasing annealing time. Figure 30 shows the relative $^{16}O^-$ on intensity profiles obtained at the back surface after damage introduction (no annealing) and after annealing at variable temperatures for 64 and 72 hrs. Also included for reference is the *measured* dislocation line density as a function of depth beneath damage grooves.

After annealing at 300°C for 64 hrs., oxygen is concentrated within a zone < 2-μm wide at the back side of the wafer. When the temperature is increased to 350°C, the gettered oxygen is distributed over a region extending 8.0 μm below damage grooves at the back surface. After annealing at 400°C or 500°C for periods >64 hrs., additional gettering of oxygen is noted throughout the damage region, resulting in a graded concentration profile that reflects the decreasing dislocation line density with increasing depth from the back surface. In comparative tests on vacuum annealed samples and samples annealed in flowing Ar, no essential difference in the distribution of gettered oxygen is observed in the profiles obtained, suggesting that the annealing process is not a significant oxygen source in these experiments.

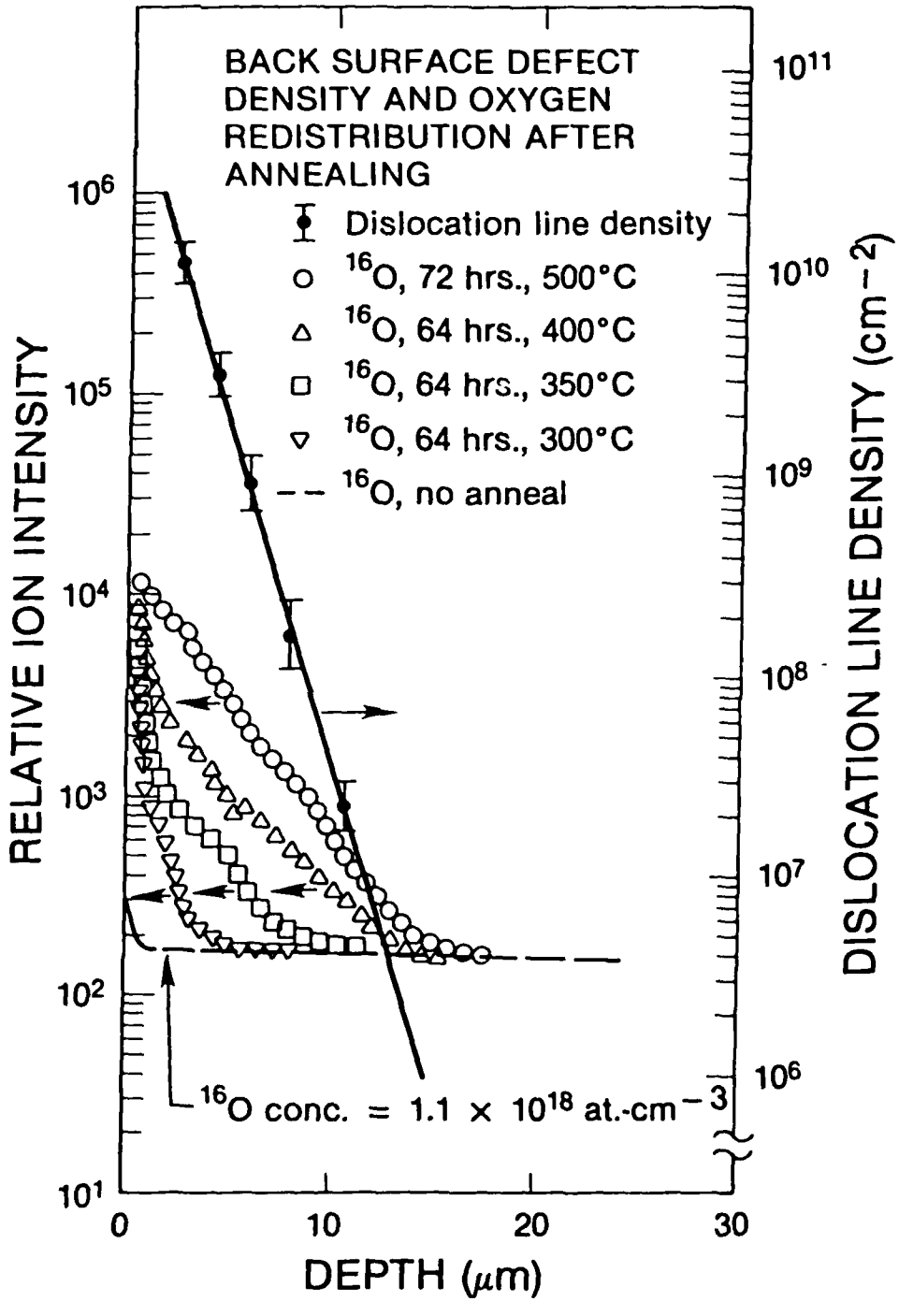

FIG. 30. BACK-SURFACE DEFECT DENSITY AND SIMS PROFILES OF RELATIVE ^{16}O ION INTENSITIES AFTER ANNEALING AT VARIABLE TEMPERATURES.

Figure 31, shows a semilog plot of the gettered ^{16}O content as a function of $10^3/T(°K)$ for samples annealed for 48 and 72 hrs. at variable temperatures. The amount of gettered oxygen was obtained by integrating the oxygen concentration profiles over the gettering depth, relative to the back surface, with the limit of integration set at the point where the oxygen (gettered) profile intersects the background or bulk oxygen doping level ($1.1 \times 10^{18}/cm^3$). Using the data shown in Fig. 31, an activation energy of 0.92 ± 0.04 eV was computed.

The above data indicate that oxygen is rapidly redistributed and gettered by back-surface damage at temperatures as low s 300°C. The process can be characterized by an activation energy of 0.92 eV in the presence of a large stress field provided by the vertically-graded dislocation-line density at the wafer backside. Both transmission electron and secondary ion micrographs confirm the presence of oxygen-related (SiOx) precipitates along dislocation lines. Correlated SIMS profiles also show a graded oxygen profile indicative of the decreasing dislocation line density as a function of depth.

From these data, the possibility of enhanced motion of the oxygen via a dislocation line/pipe diffusion mechanism can be negated, since transport along a diffusion pipe would not result in a graded oxygen profile. Furthermore, the flux of oxygen atoms moving from the interior of the wafer to the backside would require an additional driving force for accelerated mass transport.[13] Hence, it appears that the low-temperature diffusion and gettering of oxygen observed in these experiments is largely controlled by the magnitude of the stress gradient at the back surface. It can be speculated that similar low-temperature diffusion of oxygen will occur in the presence of a stress field, regardless of whether such fields are introduced by ion implantation damage, precipitation or contact alloying.

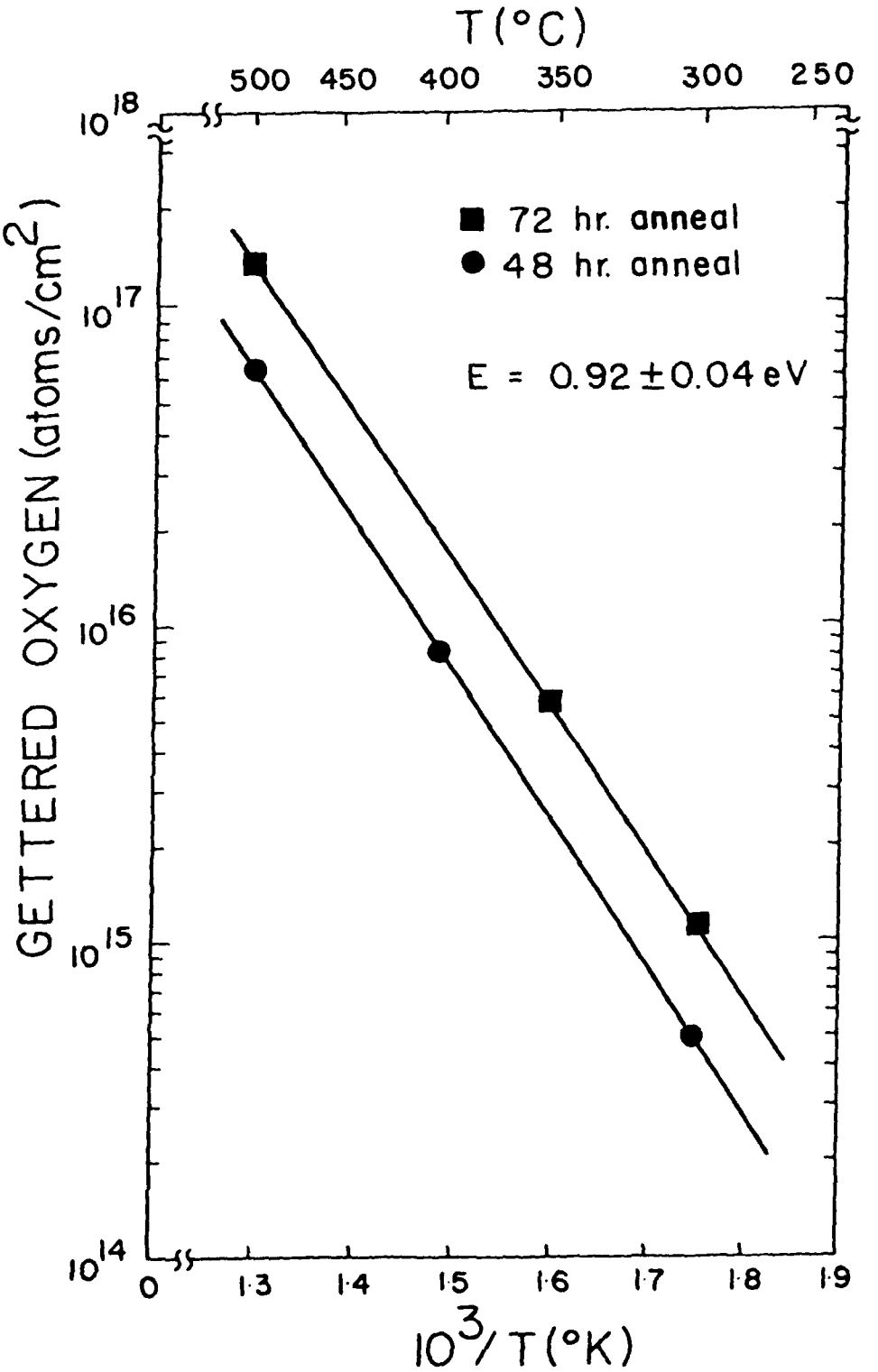

FIG. 31. BACK-SURFACE-GETTERED ^{16}O CONCENTRATIONS VS. RECIPROCAL TEMPERATURE FOR 48- AND 72-HR. ANNEALING PERIODS.

A number of investigations[14-18] have shown that various double-annealing schedules can be employed to induce internal SiOx precipitation that is effective in trapping of impurities during processing. Recent experiments using two-step annealing of back-surface-damaged wafers and the rapid diffusion and gettering of oxygen to stabilize damage have shown that extrinsic gettering is effective for extended periods of time at temperatures $\geq$ 1000°C[12]. Using the two-step-annealing schedule stabilizes back-surface damage and induces internal SiOx nucleation, so that both stabilized extrinsic and intrinsic gettering are present. However, the stabilized back-surface structure should exert some influence on SiOx nucleation and gettering within the interior of the wafer. In this section, we report on the effect of back-surface damage in two-step annealing on SiOx nucleation and front-surface-defect denudation zones using correlated data from transmission electron microscopy (TEM), scanning electron microscopy (SEM), optical microscopy, secondary ion mass spectrometry (SIMS) profiling, and secondary ion microscopy measurements. Samples used in these studies were n-type, 75-mm-diameter Czochralski (CZ)-Si wafers of [100] orientation and $\sim$ 500-μm thickness. Preliminary estimates of background oxygen concentrations on as-received wafers were made using Fourier transform infrared absorption techniques and ASTM procedures. From these measurements, average oxygen concentration of $1.7 \times 10^{18}/cm^3$ was determined.

In one set of experiments, wafers were polished on both sides and subjected to thermal annealing treatments. Separate lots of wafers were subjected to back-side mechanical abrasion[8,9,12] to introduce defect distributions at one surface,

prior to annealing. Primary and secondary annealing were performed in a flowing Ar environment at 600°C for periods of 3 to 24 hrs.and at 1050°C for periods of 3 to 6 hrs., respectively. Subsequent oxidation of selected wafers was done at 1100° in dry O_2 for a period of 4.5 hrs.

Specimens for vertical-cross-section TEM analysis were prepared by cutting thin strips along <110> directions and potting in EPON 812, as described in an earlier publication[12]. Ion milling was then used to obtain thin regions at various depth locations for examination in the electron microscope.

In-depth profiling of oxygen concentration was performed using a Cameca IMS-3f ion microanalyzer employing Cs^+ ion bombardment and negative secondary ion mass spectrometry for control and back-surface-damaged samples. In all cases, calibration of ^{16}O concentrations were obtained using standards prepared by ion implanting ^{16}O into CZ and float zone Si. Samples for secondary ion microscopy[10] analysis in vertical cross-section were prepared by mounting thin strips cut along a <110> direction in a low-melting-point Sn-Bi alloy, as described earlier.[12]

After double annealing of back-surface-damaged wafers (600°C, 3 to 24 hrs + 1050°C, 3 to 6 hrs.), TEM analysis of back-surface regions showed the presence of a stabilized defect distribution and significant SiOx nucleation within forested dislocation line regions in primary and secondary zones at the back surface, consistent with previously reported results[7,8]. Examination of vertical cross sections, prepared after double annealing and oxidation, showed the presence of SiOx precipitates distributed within the interior of the Si, as shown in Fig.32. Similarly, in samples containing no back-surface damage and subjected to identical annealing, we observed comparable SiOx internal nucleation and defect generation.

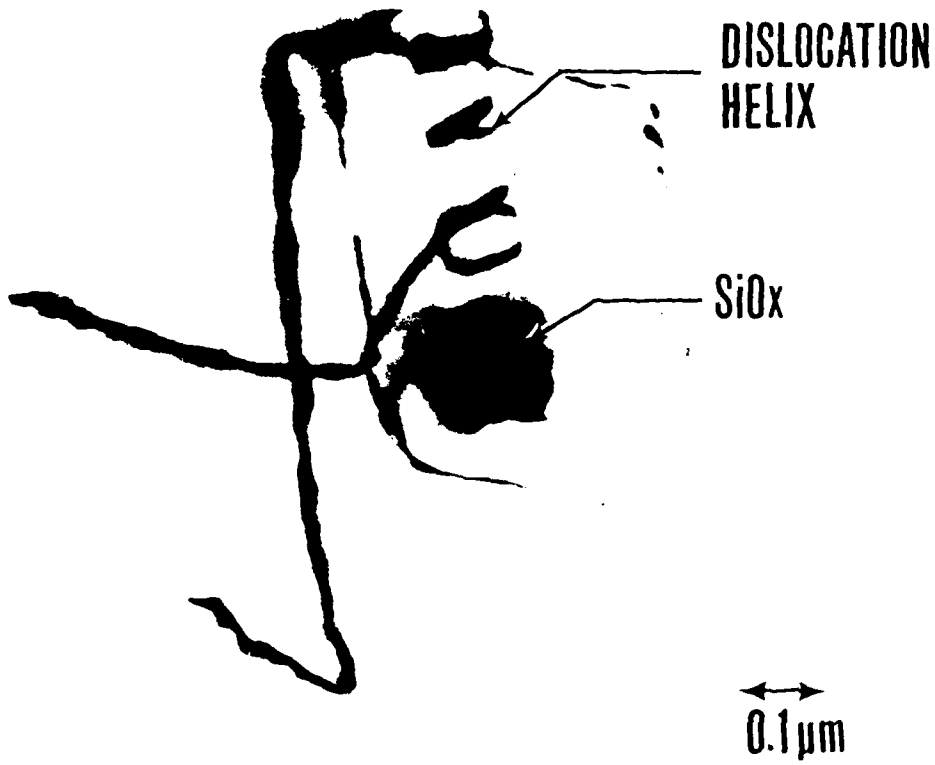

FIG. 32. VERTICAL-CROSS-SECTION ((110) PLANE) ELECTRON MICROGRAPH OBTAINED WITHIN THE INTERIOR OF DOUBLE-ANNEALED, BACK-SURFACE-DAMAGED WAFER. DISLOCATION HELICES AND LINE STRUCTURE ARE OBSERVED AT THE EDGE OF THE SiOx PERCIPITATE.

In both cases, an apparent SiOx denudation region could be observed at the front surface. However, after 600°C, 24 hr. + 1050°C, 3-hr. annealing of samples containing no back-surface damage, we observed a defect denudation width of 45 μm, whereas in comparably annealed back-surface-damaged samples, a maximum denudation width of $\simeq$ 170 μm was detected.

In subsequent experiments in which the 600°C annealing time was varied from 3 to 24 hrs. on back-surface-damaged samples, we observed an increasing defect denudation width as a function of primary anneal duration. Correlated secondary ion micrographs obtained in vertical cross section confirmed the presence of SiOx precipitates nucleated within the interior of the wafer. The data showed a relative absence of pronounced precipitation at the surface, with the width of the denuded region increasing as a function of primary annealing time at 600°C on back-damaged samples.

To obtain further information on the distribution of internal SiOx precipitation and associated defect sites, samples were cleaved along a <110> direction following double-phase annealing and oxidation for 4.5 hrs. After immersion in a modified Secco solution, we obtained optical micrographs of the etched surfaces. Single anneals at 600°C were found to produce precipitation sites distributed throughout the wafer, whereas separate 3-hr. anneals at 1050°C resulted in only a small density of observable precipitates, in agreement with earlier reported data.[16]

After annealing of (two-sides polished, no back-surface damage) samples at 600°C (12 hrs.), followed by a 1050°C (3 hr.) anneal (Fig. 33a), internal defect-free zones of $\simeq$ 45-μm width were present at both surfaces. In Figs. 33b) and 33c), the effective width of the denudation zone at the front surface is

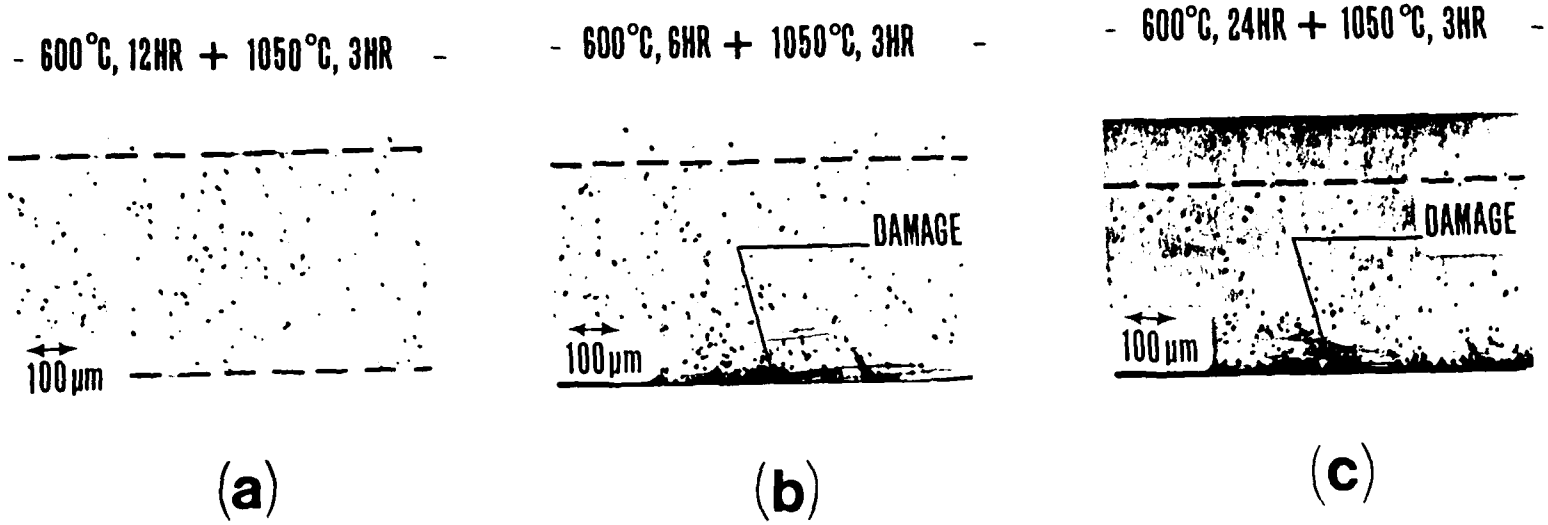

FIG. 33. OPTICAL MICROGRAPHS OBTAINED ON (110) PLANE ON DOUBLE-ANNEALED SAMPLES AFTER MODIFIED SECCO ETCHING. FRONT-SURFACE DEFECT DENUDATION ZONES ARE SHOWN FOR EACH CASE. THESE REGIONS ARE CHARACTERIZED BY A RELATIVE ABSENCE OF EXCESSIVE SiOx NUCLEATION.

increased in double-annealed, back-damaged samples, in agreement with the secondary ion microscopy data. It is important to note that both the denudation width and spatial distribution /density of internal precipitation sites is influenced by the annealing conditions, suggesting that the stabilized back-surface-damage region is controlling both oxygen diffusion and SiOx nucleation site stability.

To ascertain any possible correlation between oxygen outdiffusion and defect denudation zones at the front surface, we obtained SIMS profiles of the oxygen concentrations, in control (*no anneal*) and annealed samples. In Fig. 34, we show that annealing of either back-surface-damaged or double-side-polished (no damage) wafers at 600°C for 24 hrs. produces no significant outdiffusion of oxygen, with only a slight depletion occuring at the surface. Annealing at 1050°C produces a well-defined oxygen depletion region ($\underset{\sim}{}$ 17 μm) for both damaged and undamaged wafers. In comparison, we observe that doubly-annealed (600°C + 1050°C) wafers exhibit an outdiffusion profile that is essentially identical to the profile obtained after a single anneal at 1050°C. The results then show that the primary anneal at 600°C has little or no effect on the outdiffusion profile obtained after secondary high-temperature anneals. For reference, we also show the oxygen profile obtained after a 450°C, 64-hour anneal, indicating that no significant oxygen depletion occurs after low temperature annealing in the absence of defects. This is in sharp contrast to recent results which indicate that in the presence of defects, enhanced diffusion of oxygen occurs even at temperatures as low as 350°C.[19]

In Figure 35, shows graphically the (front-surface) oxygen and defect denudation widths as a function of 600°C primary

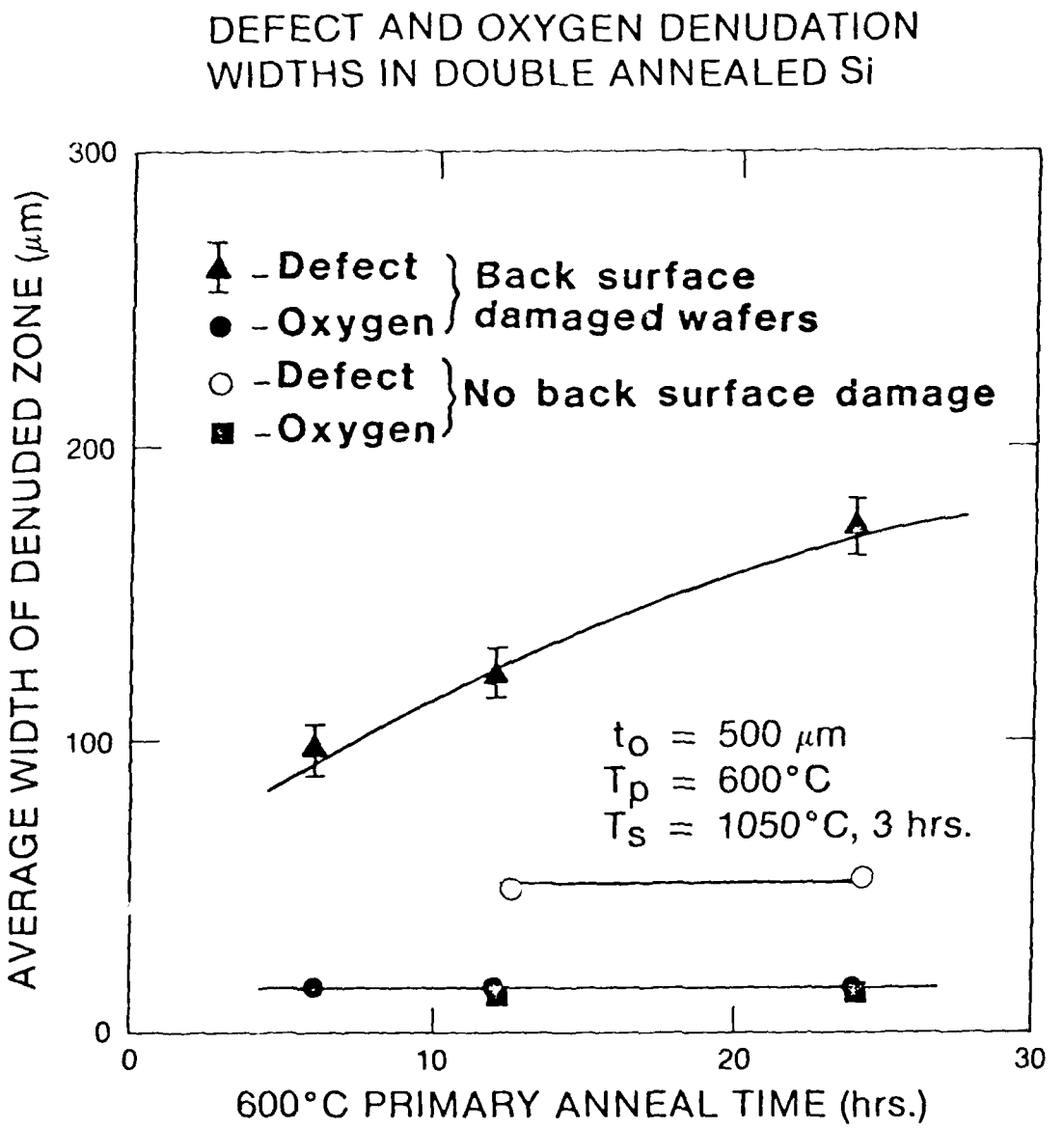

FIG. 35 DEFECT AND OXYGEN DENUDATION WIDTHS IN DOUBLE-ANNEALED SAMPLES AS A FUNCTION OF PRIMARY ANNEAL (T_p = 600°C) DURATION IN WAFERS SUBJECTED TO 600°C + 1050°C (3 HR.) ANNEALING TREATMENT. RESULTS ON BOTH DOUBLE-SIDE POLISHED AND BACK-SURFACE-DAMAGED ANNEALED WAFERS ARE SHOWN. WAFER THICKNESS, T_o = 500 μm.

anneal time on double-annealed (600° + 1050°C, 3 hr) back-surface-damaged samples. Also shown are the corresponding denudation widths obtained on double-side-polished wafers subjected to similar anneals. The data shows no significant correlation between the width of defect denudation regions and oxygen depletion regions at the front surface, as anticipated. As the primary anneal time at 600°C is increased, a dramatic increase in the width of the defect denudation zone is observed, approaching relative saturation at anneal times $\geq$24 hrs. Under the experimental conditions utilized, where the secondary high-temperature anneal is constant (3 hrs.), the width of the oxygen depletion region is invariant to changes in low-temperature primary anneal duration.

From the data obtained, we can conclude that the primary anneal duration influences the spatial distribution of SiOx nucleation within the interior of back-surface-damaged, double-annealed wafers. Since the duration of the 600°C primary anneal will influence the amount of oxygen diffusing to back-surface-damage regions, the stabilization of primary defects and secondary damage zones will be effected in subsequent high-temperature processing. Also, the effective gettering of impurities and defects depends on the magnitude of the effective stress field at the back surface. Thus, increases in the 600°C anneal time result in the creation of larger stress fields induced as a result of the increases in back-surface-damage densities during high-temperature secondary annealing.

The present experiments suggest that the stabilized back-surface damage will be effective in gettering of internal impurity or defect sites that serve as cluster zones for SiOx nucleation. However, additional research is required to identify both the nature of these nucleation sites and the kinetics of SiOx nucleation in the presence of stabilized back-surface-damage structure and enhanced long-range oxygen diffusion.[12]

The control of SiOx nucleation by (stabilized) back-surface-damage will depend on initial quality of starting material, anneal conditions, method of back-surface-damage introduction and a number of other processing-related factors, which will vary between various laboratories. The results reported do not necessarily propose an optimal procedure for control of denudation zones and internal SiOx nucleation, but simply point out that in the presence of a stable back-surface-gettering region, created by two-step annealing, spatial control of both nucleation sites and precipitation can be accomplished.

5. CONCLUSIONS

The data obtained in this program, suggests that the quality of Si wafers currently used by device manufacturing facilities in the U.S. is extremely variable. The majority of the wafers examined in this program were obtained directly from line runs where the wafers had been previously accepted and qualified for facility usage. Thus, the data point-out the current lack of standards or uniformly developed industry criteria for qualification of wafers to be used in device fabrication.

Of equal importance is the lack of consistent quality in material from various suppliers. Although Si wafers provided separately by suppliers were found to be acceptable, the statistical sampling of wafers currently provided for mass production facilities shows that much of the material currently used by device manufacturers would probably be unacceptable for VHSIC fabrication.

Additional experiments on the use of gettering has shown that the quality of wafers can be improved if stabilized damage is present. Since damage introduced by ion implantation, mechanical damage or P-diffusion is largely annihilated after single, short-term, high-temperature anneals, the use of two-phase anneal-stabilization procedures is essential.

These studies also identified the rapid redistribution of oxygen in the presence of defects. Since the microscopic, not the bulk, redistribution of oxygen in Si is the most important factor for VHSIC processing, the enhanced diffusion and gettering of background oxygen into defect regions produced during processing will be a critical factor for future integrated circuit technology.

6. REFERENCES

1. Annual Book of ASTM Standards (ASTM, Philadelphia, 1977) F-121.

2. F. Secco d' Aragona, J. Electrochem. Soc.119, 948(1972).

3. V.E. Sirtl and A.M. Adler, Z. Metallk. 52H, 529(1961).

4. C. Synborski, Solid State Tech.20 (June,1980).

5. L.J. Palkuti, J. Peng, C. Welles and T.C. Teng, Proceedings of the 30th Electronic Components Conference, IEEE Cat. No. 80, Ch. 1568-5, 37(1980).

6. K. Hoshi, T. Suzuki, Y. Okubo and N. Isawa, Proc. Electrochem. Soc. Symposium, Spring, 1980, St. Louis, Mo. (Electrochem. Soc., Princeton, N.J.).

7. C. Cohen, Electronics, p. 83, July 3, 1980.

8. J.E. Lawrence, Met. Soc. AIME 242, 484 (1968).

9. T.J. Magee, J. Peng, J.D. Hong, W. Katz and C.A. Evans, Jr., Phys. Stat. Sol.(A) 55, 161(1979).

10. G.H. Morrison and G. Slodzian, Anal. Chem. 47, 932A (1975).

11. S.M. Hu, Appl. Phys. Lett. 31, 53(1977).

12. T.J. Magee, C. Leung, H. Kawayoshi, B.K. Furman and C.A. Evans, Jr., Appl. Phys. Lett. 38, 891(1981).

13. P.G. Shewman, Difffusion in Solids (McGraw-Hill, New York, 1971), Chap. 1.

14. T.Y. Tan, E.E. Gardner and W.K. Tice, Appl. Phys. Lett. 30, 175(1975).

15. S. Kishino, S. Isomae, M. Tamura and M. Maki, Appl. Phys. Lett. 32, 1(1978).

16. K. Yamamoto, S. Kishino, Y. Mashushita and T. Iizuka, Appl. Phys. Lett. 36, 195(1980).

17. S. Kishino, M. Kanamori, N. Yoshihiro, M. Tajima and T. Iizuka, Appl. Phys. 50, 8280(1979).

18. F. Shimura, H. Tsuya and T. Kawamura, Appl. Phys. Lett. 37, 483(1980).

19. T.J. Magee, C. Leung, H. Kawayoshi, B.K. Furman and C.A. Evans, Jr., J. Appl. Phys. 52, 5392(1981).

DISTRIBUTION LIST

	Addressee	Copies
1)	Scientific Officer Office of Naval Research	1
2)	Administrative Contracting Officer DCASMA-San Francisco 1250 Bayhill Drive San Bruno, CA 94066	1
3)	Director Naval Research Laboratory Washington, D.C. 20375 Attn: Code 2627	6
4)	Defense Documentation Center Bldg. 5, Cameron Station Alexandria, VA 22314	12
5)	Pasadena Branch Office Office of Naval Research 1030 East Green Street Pasadena, CA 91106	1